Supplementary information for:

Extreme promiscuity of a bacterial and a plant diterpene synthase enables combinatorial biosynthesis

Meirong Jia, Kevin C. Potter and Reuben J. Peters

Roy J. Carver Department of Biochemistry, Biophysics & Molecular Biology, Iowa State University, Ames, IA 50011, USA

Contents

Table S1: Vectors used in this study.

Vector	Marker	Gene(s)/cassette	Origin	Reference
pIRS	Spec	idi, dxr, dxs	pCDFDuet	(Morrone et al., 2010)
pGG	Chlor	GGPPS	pACYCDuet	(Cyr et al., 2007)
pGG-DEST	Chlor	GGPPS, DEST cassette	pACYCDuet	(Morrone et al., 2010)
pGG-DTCs[a]	Chlor	GGPPS, DEST::DTCs	pACYCDuet	This study
pGG-DTSs[a]	Chlor	GGPPS, DEST::DTSs	pACYCDuet	This study
pDEST	Amp	DEST cassette	pBR322	Thermo Fisher Scientific
pDEST-DTSs	Amp	DEST::DTSs	pBR322	(Morrone et al., 2010)
NNPP	Amp	NNPPS	pEXP5-CT/TOPO	(Matsuba et al., 2015)
NNPP-DEST	Amp	NNPPS, DEST cassette	pEXP5-CT/TOPO	This study
NNPP-DTSs	Amp	NNPPS, DEST::DTSs	pEXP5-CT/TOPO	This study

[a]All DTCs used in this work (i.e., listed in Table 1) were inserted into the pGG-DEST vector, except KgTPS, which was put into the pDEST vector, with the paired DTSs inserted into the pGG-DEST vector for co-expression.

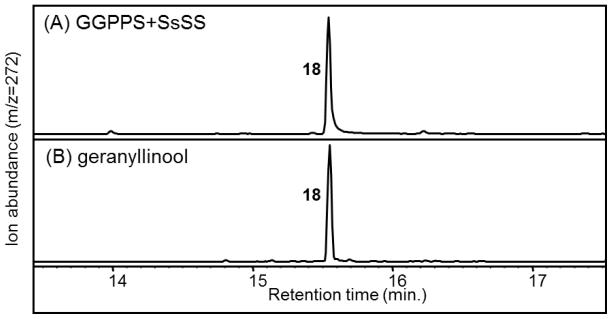

Fig. S1. GC-MS chromatograms of extracts from *E. coli* engineered for production of GGPP (**1**) by co-expressing GGPPS with SsSS (A), geranyllinool standard (B), obtained from Prof. Tholl from Virginia Tech (Herde et al., 2008). Mass spectra for various peaks in the chromatograms in Fig. 2. (C) **15**: β-springene; (D) **16**: (*Z*)-α-springene; (E) **17**: (*E*)-α-springene; (F) **18**: geranyllinool; (G) authentic geranyllinool (**18**, peak in panel B).

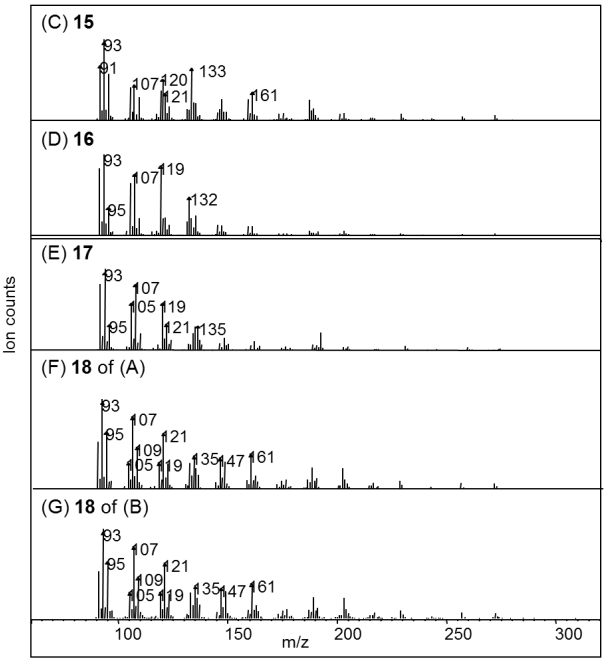

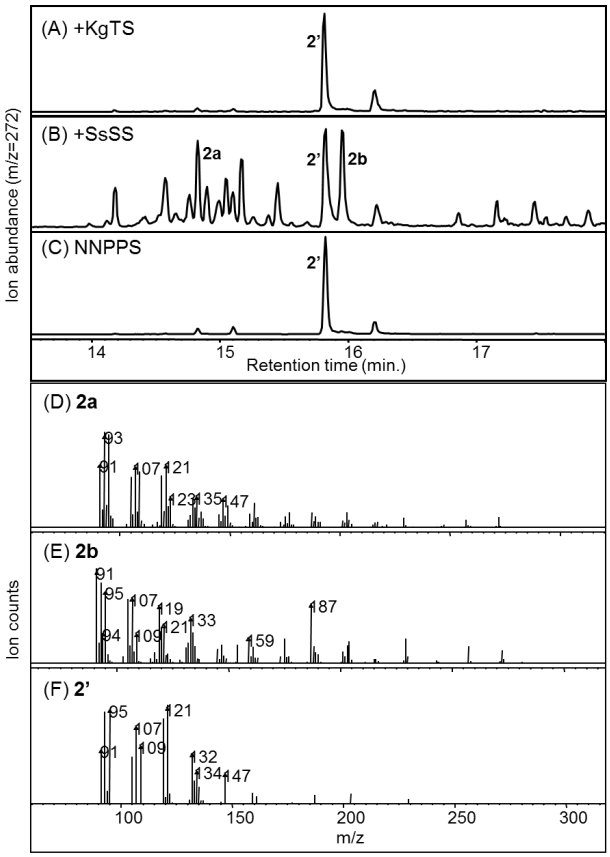

Fig. S2. GC-MS chromatograms of extracts from *E. coli* engineered for production of NNPP (**2**) by co-expressing NNPPS (C) with KgTS (A) or SsSS (B). Mass spectra for respective peaks in the chromatograms. (D) **2a**: putative diterpene **2a**; (E) **2b**: putative diterpene **2b**; (F) **2'**: the dephosphorylated derivative of **2** (nerylnerol). Note: At this stage, it was not possible to isolate sufficient amounts of these products for structural determination of compounds **2a** and **2b**.

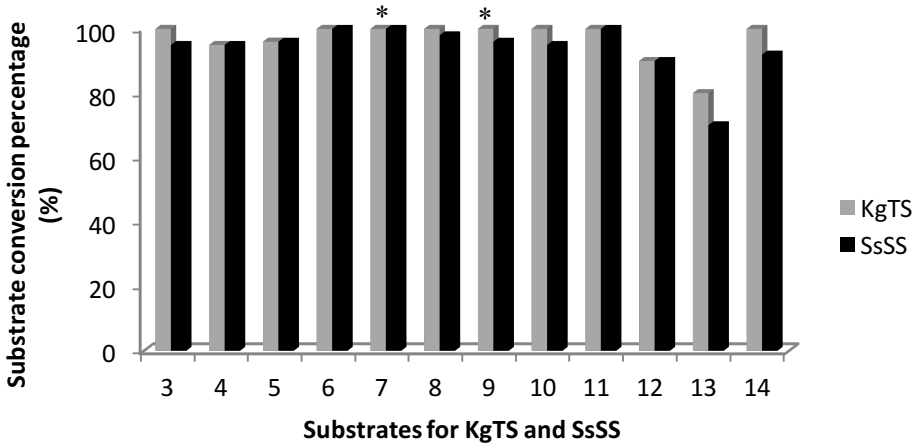

Fig. S3. The substrate conversion percentages of both KgTS and SsSS towards all the 12 bicyclic substrates (Numbers correspond to chemical structures defined in text and previous Fig. legends). * Indicate **7** and **9** as the native substrates of SsSS and KgTS, respectively.

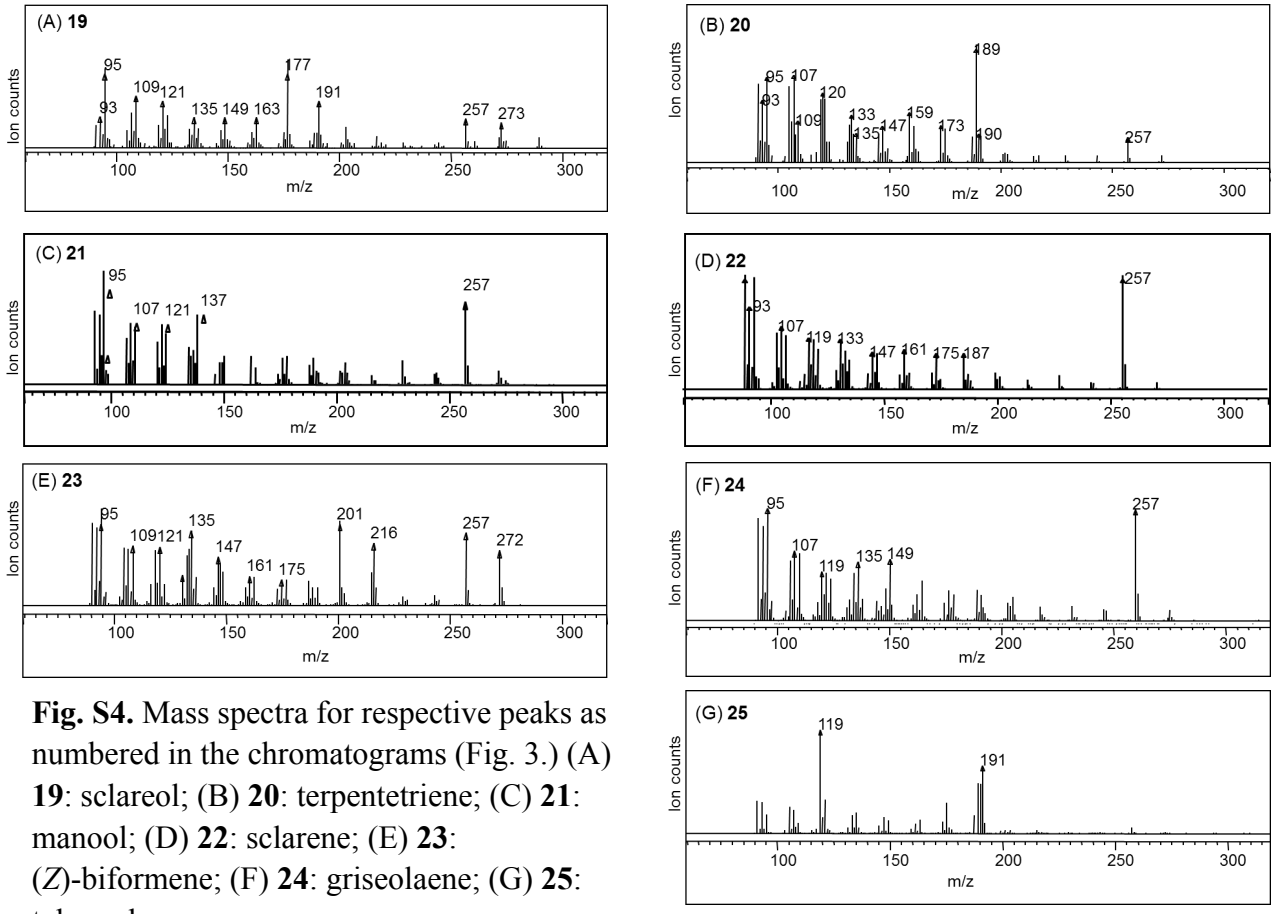

Fig. S4. Mass spectra for respective peaks as numbered in the chromatograms (Fig. 3.) (A) **19**: sclareol; (B) **20**: terpentetriene; (C) **21**: manool; (D) **22**: sclarene; (E) **23**: (*Z*)-biformene; (F) **24**: griseolaene; (G) **25**: tuberculosene.

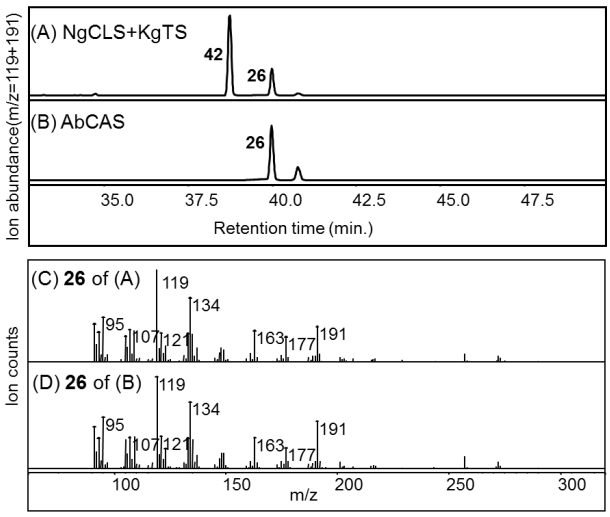

Fig. S5. Chromatograms from GC-MS analysis of extracts from *E. coli* engineered for production of 8α-hydroxy-CPP (**7**) by co-expressing NgCLS with KgTS (A) (numbering as defined in the text, with **7'** corresponding to the dephosphorylated derivative of **7**). Mass spectra for indicated peaks (C)/(D) **26**: *cis*-abienol. SsSS product was identified by comparison (both retention time and mass spectrum) to the same product produced by the bi-functional (DTC/DTS) *cis*-abienol synthase AbCAS (B) (Zerbe et al., 2012).

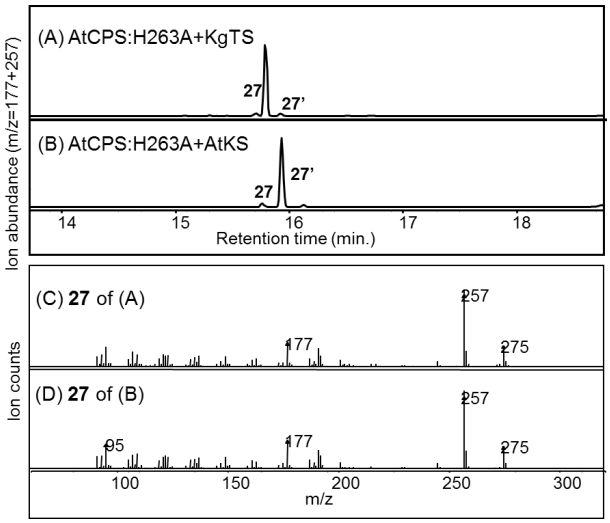

Fig. S6. Chromatograms from GC-MS analysis of extracts from *E. coli* engineered for production of 8β-hydroxy-*ent*-CPP (**8**) by co-expressing AtCPS:H263A with KgTS (A) or AtKS (B) (numbering as defined in the text, with **8'** corresponding to the dephosphorylated derivative of **8**, and **27'** to the (13*S*)-isomer of **27**). Mass spectra for indicated peaks (C)/(D) **27**: *ent*-manoyl oxide. KgTS product was identified by comparison of both retention time and mass spectrum to the minor AtKS product (Mafu et al., 2015).

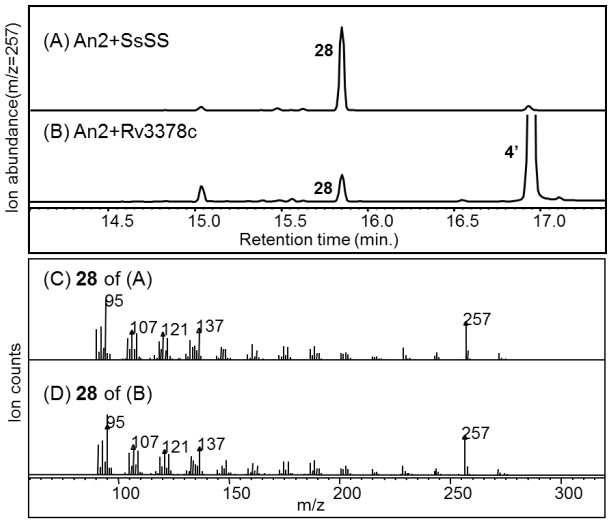

Fig. S7. Chromatograms from GC-MS analysis of extracts from *E. coli* engineered for production of *ent*-CPP (**4**) by co-expressing An2 with SsSS (A) or Rv3378c (B) (numbering as defined in the text, with **4'** corresponding to the dephosphorylated derivative of **4**). Mass spectra for indicated peaks (C)/(D) **28**: *ent*-manool. SsSS product was identified by comparison (both retention time and mass spectrum) to the known Rv3378c product (Hoshino et al., 2011).

Fig. S8. Chromatograms from GC-MS analysis of extracts from *E. coli* engineered for production of *syn*-CPP (**5**) by co-expressing OsCPS4 with SsSS (A) or Rv3378c (B) (numbering as defined in the text, with **5'** corresponding to the dephosphorylated derivative of **5**). Mass spectra for indicated peaks (C)/(D) **29**: vitexifolin A. SsSS product was identified by comparison (both retention time and mass spectrum) to the known Rv3378c product (Hoshino et al., 2011).

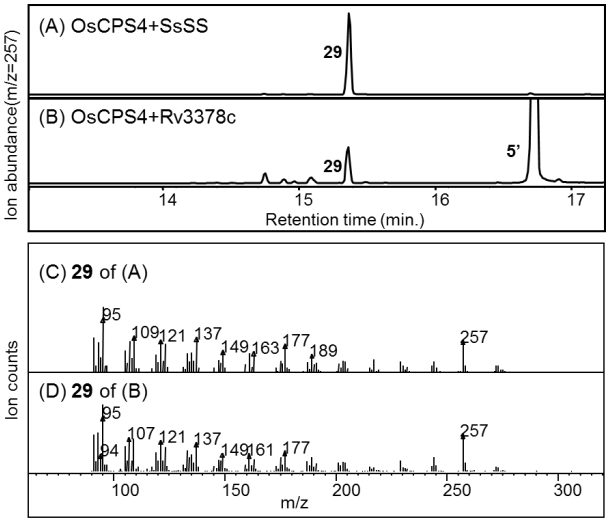

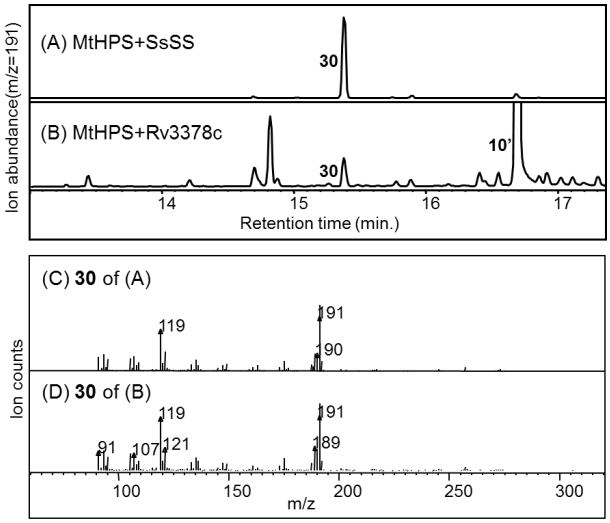

Fig. S9. Chromatograms from GC-MS analysis of extracts from *E. coli* engineered for production of tuberculosinyl diphosphate (**10**) by co-expressing MtHPS with SsSS (A) or Rv3378c (B) (numbering as defined in the text, with **10'** corresponding to the dephosphorylated derivative of **10**). Mass spectra for indicated peaks (C)/(D) **30**: isotuberculosinol. SsSS product was identified by comparison (both retention time and mass spectrum) to the known Rv3378c product (Hoshino et al., 2011).

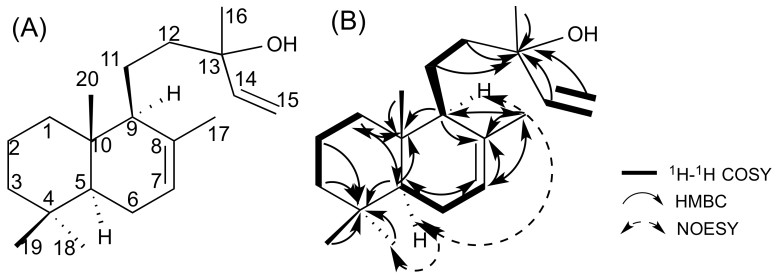

(9*R*,10*S*)-labda-7,14-dien-13-ol (**31**)

Fig. S10. The product of SsSS co-expressed with SmCPS/KSL1:D500A/D504A. (A) Numbering; (B) ^{1}H-^{1}H COSY correlations, selected HMBC correlations and NOESY Nuclear Overhauser Effect dipole-dipole correlations used to assign the structure.

Table S2: ^{1}H and ^{13}C NMR assignments for compound **31**, (9*R*,10*S*)-labda-7,14-dien-13-ol (solvent $CDCl_3$).

Position	(9*R*,10*S*)-labda-7,14-dien-13-ol (**31**)	
	δ_H	δ_C
1 a	1.84 (1H, m)	39.4
b	0.93 (1H, m)	
2 a	1.50 (1H, m)	19.0
b	1.41 (1H, m)	
3 a	1.38 (1H, m)	42.5
b	1.23 (1H, m)	
4		33.2
5	1.14 (1H, m)	50.4
6 a	1.94 (1H, d, *J* = 18.1 Hz)	24.0
b	1.83 (1H, m)	
7	5.35 (1H,brs)	122.5
8		135.6
9	1.54 (1H, m)	55.3
10		37.2
11 a	1.47 (1H, m)	21.4
b	1.12 (1H, m)	
12 a	1.75 (1H, td, *J* = 14.4, 6.3 Hz)	45.1
b	1.46 (1H, m)	
13		73.9
14	5.89 (1H, dd, *J* = 17.4, 10.7 Hz)	145.2
15 a	5.19 (1H, d, *J* = 17.4 Hz)	112.0
b	5.04 (1H, d, *J* = 10.7 Hz)	
16	1.27 (3H, s)	28.0
17	1.64 (3H, s)	22.4
18	0.83 (3H, s)	33.4
19	0.85 (3H, s)	22.1
20	0.73 (3H, s)	13.8

Fig. S11. (A) ^{1}H Spectrum of (9*R*,10*S*)-labda-7,14-dien-13-ol (**31**)

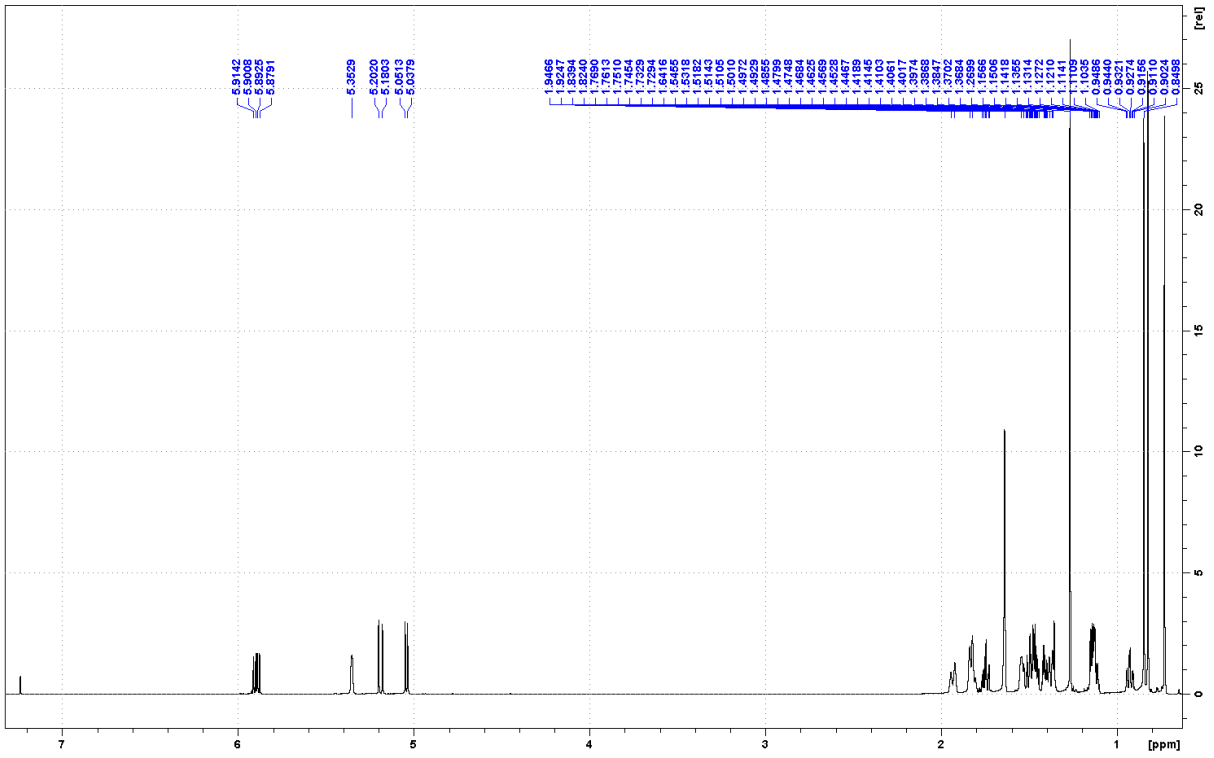

(B) ^{13}C Spectrum of (9*R*,10*S*)-labda-7,14-dien-13-ol (**31**)

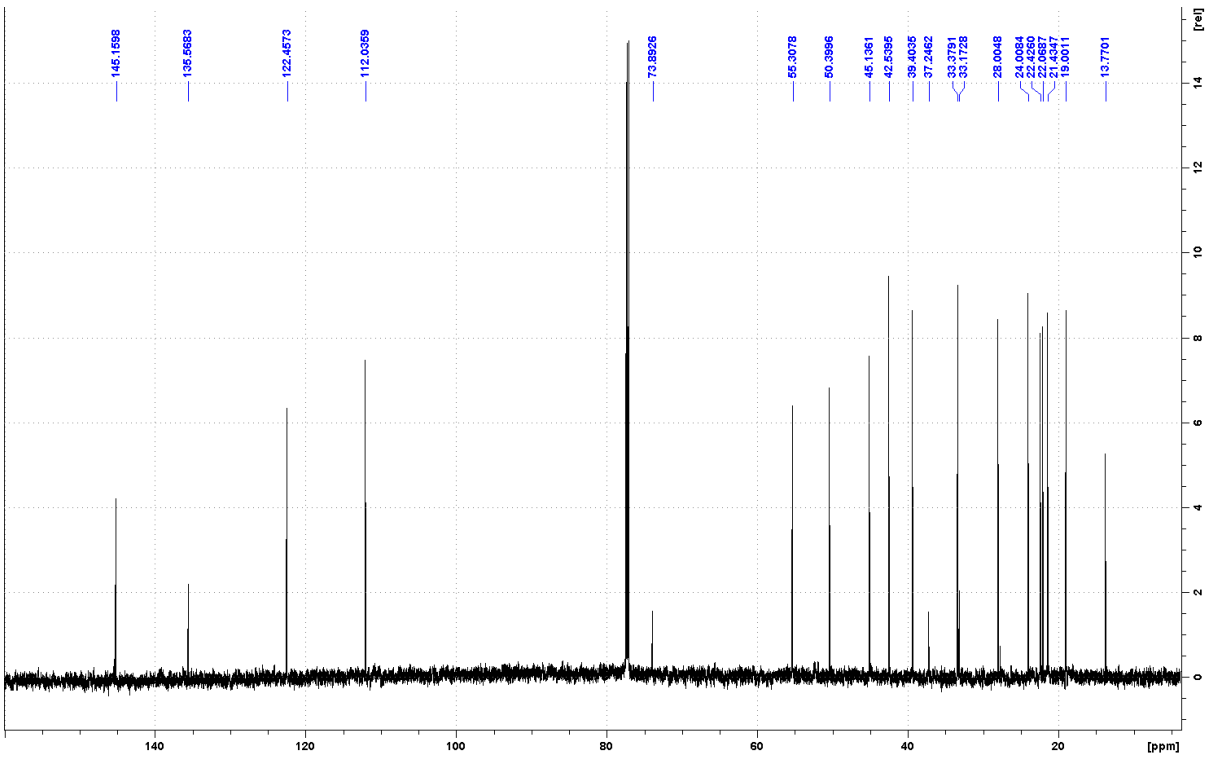

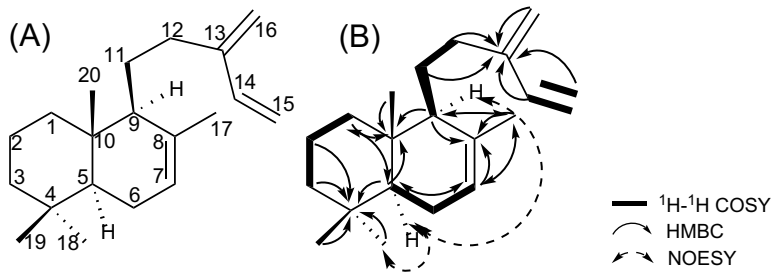

(9*R*,10*S*)-labda-7,13(16),14-triene (**32**)

Fig. S12. The product of KgTS co-expressed with SmCPS/KSL1:D500A/D504A. (A) Numbering; (B) ^{1}H-^{1}H COSY correlations, selected HMBC correlations and NOESY Nuclear Overhauser Effect dipole-dipole correlations used to assign the structure.

Table S3: ^{1}H and ^{13}C NMR assignments for compound **32**, (9*R*,10*S*)-labda-7,13(16),14-triene (solvent $CDCl_3$).

Position		(9*R*,10*S*)-labda-7,13(16),14-triene (**32**)	
		δ_H	δ_C
1	a	1.80 (1H, q, *J* = 18.1 Hz)	39.3
	b	0.94 (1H, td, *J* = 13.6, 3.5 Hz)	
2	a	1.51 (1H, m)	19.0
	b	1.41 (1H, m)	
3	a	1.38 (1H, d, *J* = 13.6 Hz)	42.5
	b	1.14 (1H, td, *J* = 13.6, 3.2 Hz)	
4			33.2
5		1.17 (1H, dd, *J* = 12.2, 4.6 Hz)	50.4
6	a	1.96 (1H, d, *J* = 18.1 Hz)	24.1
	b	1.83 (1H, m)	
7		5.38 (1H,brs)	122.5
8			135.5
9		1.66 (1H, brs)	55.1
10			37.0
11	a	1.61 (1H, m)	26.4
	b	1.32 (1H, m)	
12	a	2.43 (1H, m)	34.2
	b	2.12 (1H, m)	
13			147.3
14		6.35 (1H, dd, *J* = 17.8, 10.8 Hz)	139.1
15	a	5.23 (1H, d, *J* = 17.8 Hz)	113.4
	b	5.05 (1H, d, *J* = 10.8 Hz)	
16		4.99 (2H, d, *J* = 9.0 Hz)	116.1
17		1.66 (3H, s)	22.5
18		0.84 (3H, s)	33.4
19		0.85 (3H, s)	22.1
20		0.73 (3H, s)	13.8

Fig. S13. (A)[1]H Spectrum of (9*R*,10*S*)-labda-7,13(16),14-triene (**32**)

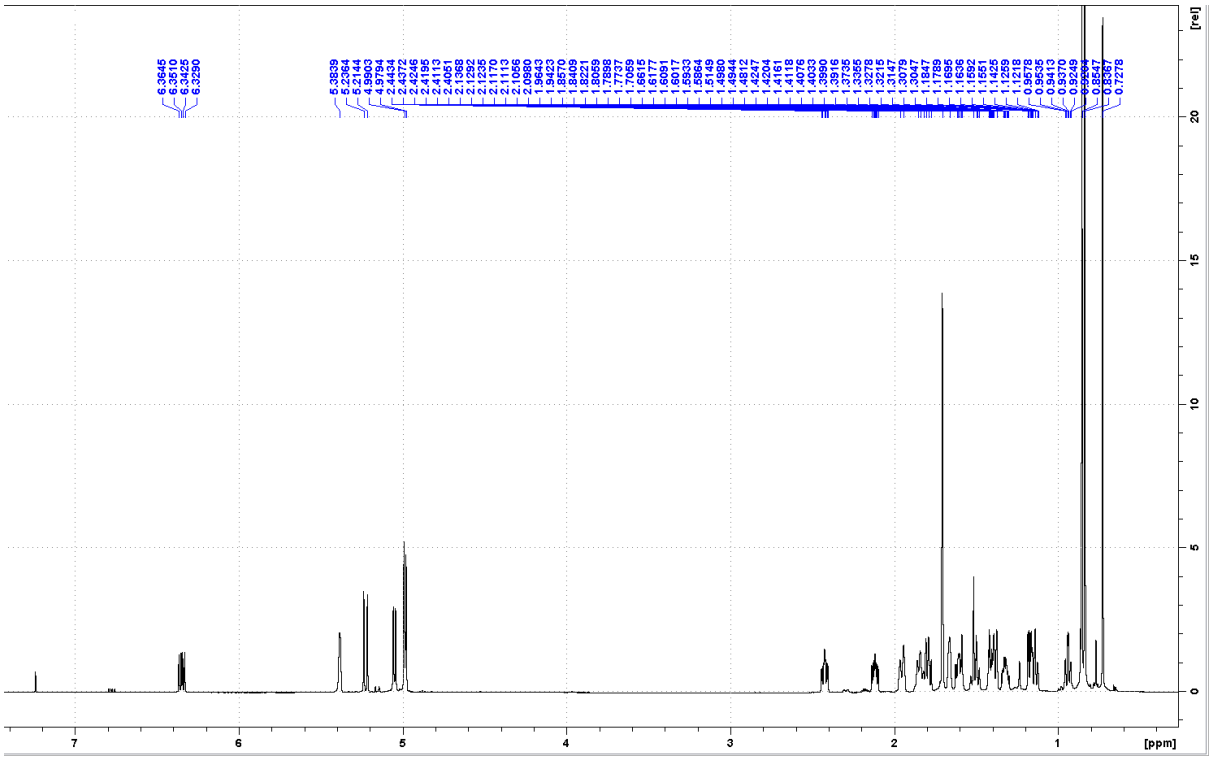

(B) [13]C Spectrum of (9*R*,10*S*)-labda-7,13(16),14-triene (**32**)

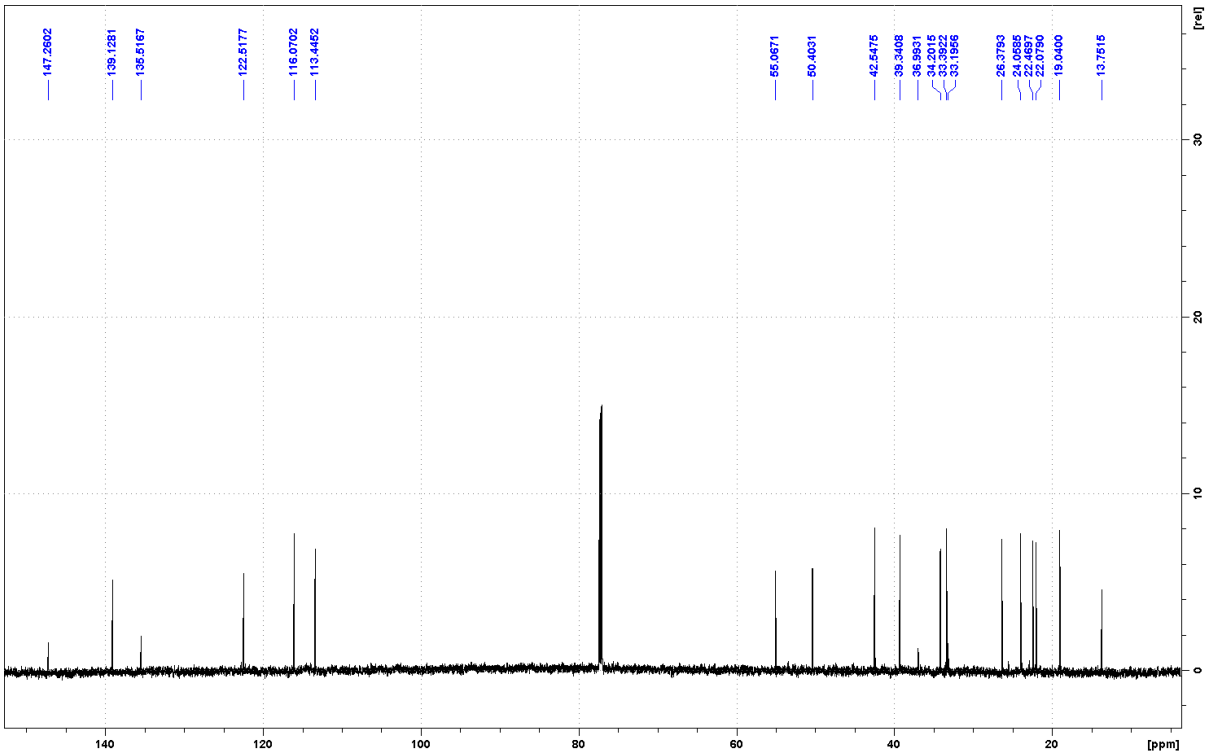

Fig. S14. Mass spectra for (A) **31**: (9*R*,10*S*)-labda-7,14-dien-13-ol; and (B) **32**: (9*R*,10*S*)-labda-7,13(16),14-triene.

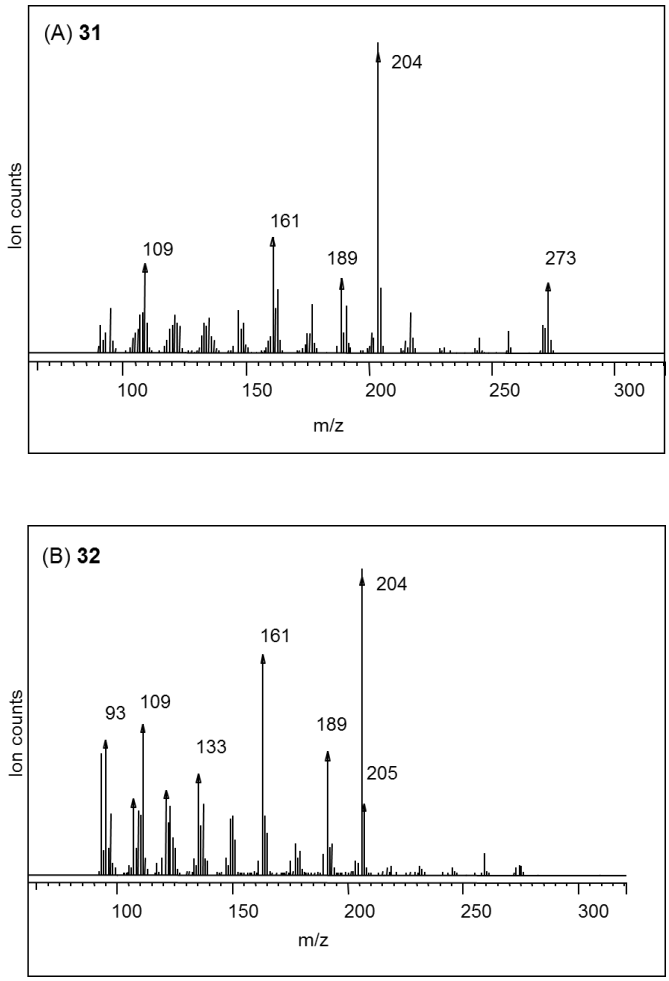

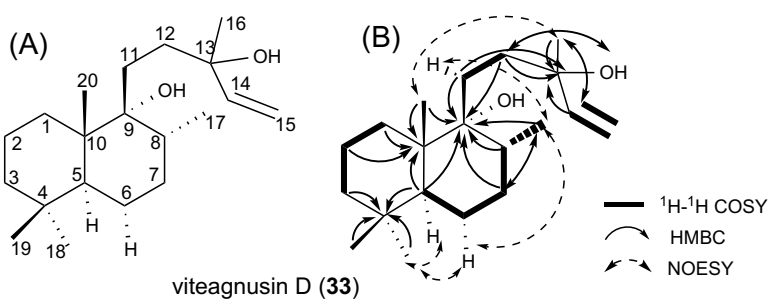

Fig. S15. The product of SsSS co-expressed with MvCPS1. (A) Numbering; (B) ^{1}H-^{1}H COSY correlations, selected HMBC correlations and NOESY Nuclear Overhauser Effect dipole-dipole correlations used to assign the structure. The C8 conformation is assigned to be *R* based on the observed NOESY correlations between H17 with H6 and H18 with H6. This assignment allows us to clarify the previously ambiguous structure of peregrinol diphosphate (Zerbe et al., 2014), which further enables us to propose that MvCPS1 generates a labda-13*E*-en-8-yl+ intermediate with *syn*- instead of normal configuration. Note: Structural characterization of viteagusin D has been previously reported (Ono et al., 2008).

Table S4: ^{1}H and ^{13}C NMR assignments for compound **33**, viteagnusin D (solvent C_6D_6).

Position		viteagnusin D (**33**)	
		δ_H	δ_C
1	a	1.58 (1H, m)	32.8
	b	1.55 (1H, m)	
2	a	1.58 (1H, m)	19.7
	b	1.52 (1H, m)	
3	a	1.38 (1H, m)	42.6
	b	1.24 (1H, m)	
4			33.9
5		1.67 (1H, dd, *J* = 12.8, 2.8 Hz)	46.8
6	a	1.54 (1H, m)	22.6
	b	1.24 (1H, m)	
7	a	1.42 (1H, m)	32.1
	b	1.37 (1H, m)	
8		1.56 (1H, m)	38.3
9			76.7
10			44.4
11	a	1.76 (1H, m)	28.9
	b	1.31 (1H, m)	
12	a	1.76 (1H, m)	37.5
	b	1.44 (1H, m)	
13			73.9
14		5.66 (1H, dd, *J* = 17.2, 10.7 Hz)	145.7
15	a	5.20 (1H, dd, *J* = 17.2, 1.66 Hz)	112.3
	b	4.99 (1H, dd, *J* = 10.7, 1.66 Hz)	
16		1.08 (3H, s)	30.0
17		0.9 (3H,d, *J* = 6.5 Hz)	17.5
18		0.93 (3H, s)	34.3
19		0.87 (3H, s)	22.6
20		0.86 (3H, s)	16.4

Fig. S16. (A) ^{1}H Spectrum of viteagnusin D (**33**)

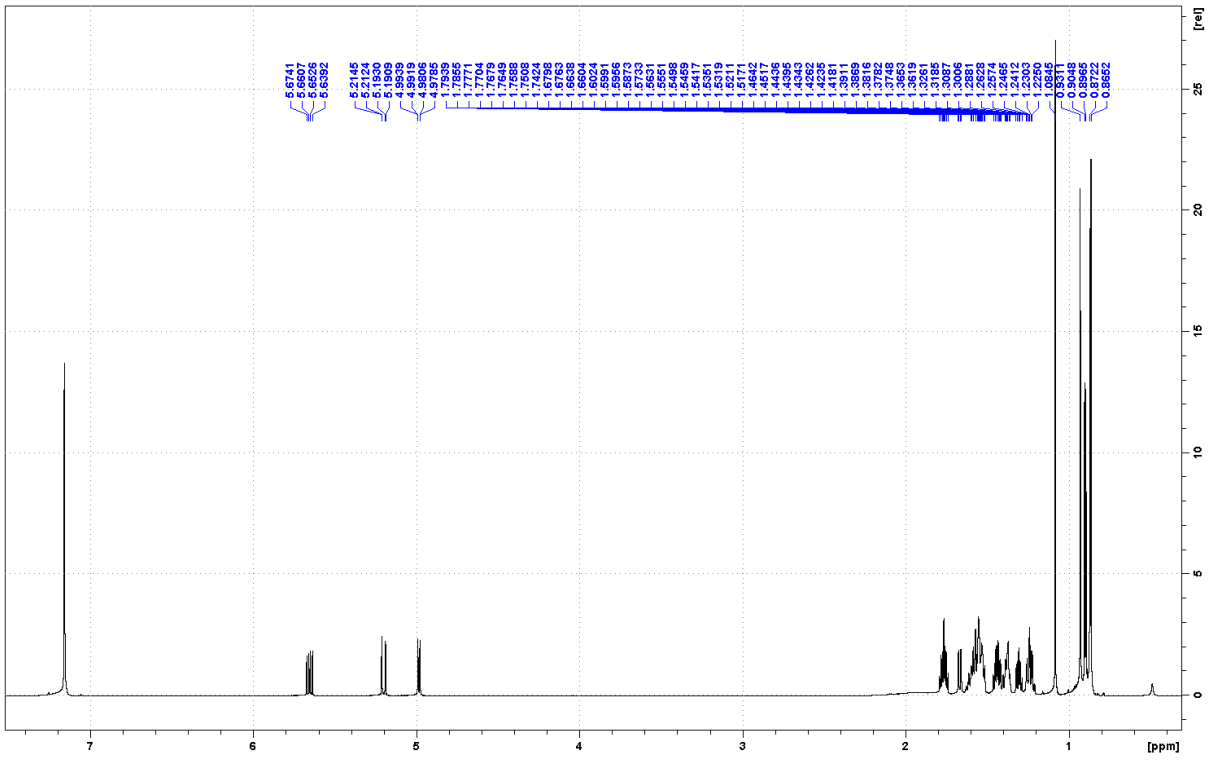

(B) ^{13}C Spectrum of viteagnusin D (**33**)

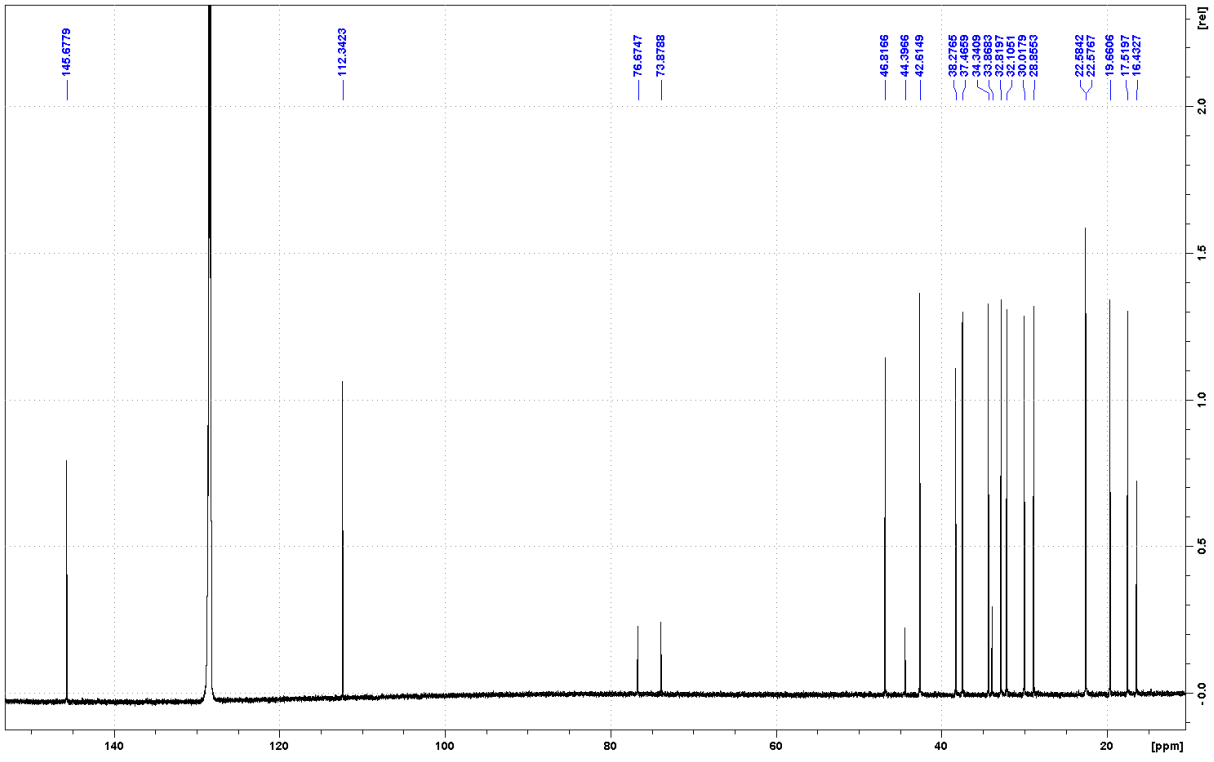

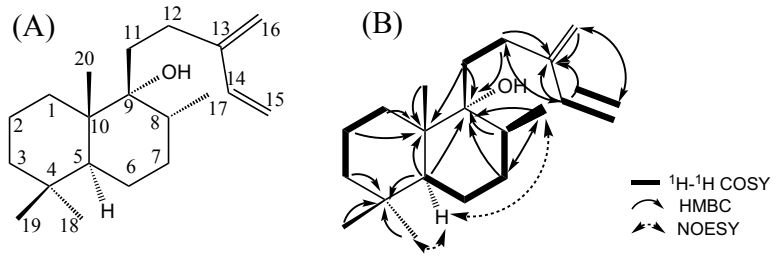

(8*R*,9*R*,10*S*)-labda-13(16),14-dien-9-ol (**34**)

Fig. S17. The product of KgTS co-expressed with MvCPS1. (A) Numbering; (B) ^{1}H-^{1}H COSY correlations, selected HMBC correlations and NOESY Nuclear Overhauser Effect dipole-dipole correlations used to assign the structure. The C8 conformation is assigned to be *R* based on the observed NOESY correlations between H17 with H5.

Table S5: ^{1}H and ^{13}C NMR assignments for compound **34**, (8*R*,9*R*,10*S*)-labda-13(16),14-dien-9-ol (solvent C_6D_6).

Position		(8*R*,9*R*,10*S*)-labda-13(16),14-dien-9-ol (**34**)	
		δ_H	δ_C
1	a	1.51 (1H, m)	32.4
	b	1.42 (1H, m)	
2	a	1.52 (1H, m)	19.4
	b	1.43 (1H, m)	
3	a	1.35 (1H, m)	42.5
	b	1.18 (1H, m)	
4			33.8
5		1.53 (1H, m)	37.4
6	a	1.47 (1H, m)	22.4
	b	1.18 (1H, m)	
7		1.42 (2H, m)	46.7
8		1.30 (1H, m)	31.9
9			77.2
10			43.9
11	a	1.82 (1H, m)	34.3
	b	1.53 (1H, m)	
12		2.34 (2H, m)	28.8
13			148.5
14		6.39 (1H, dd, *J* = 17.7, 11.3 Hz)	139.8
15	a	5.33 (1H, d, *J* = 17.7 Hz)	113.8
	b	5.03 (1H, d, *J* = 11.3 Hz)	
16		5.00 (2H, d, *J* = 18.2 Hz)	116.0
17		0.83 (3H,d, *J* = 6.5 Hz)	16.9
18		0.84 (3H, s)	22.5
19		0.9 (3H, s)	34.4
20		0.8 (3H, s)	16.6

Fig. S18. (A) ^{1}H Spectrum of (8*R*,9*R*,10*S*)-labda-13(16),14-dien-9-ol (**34**)

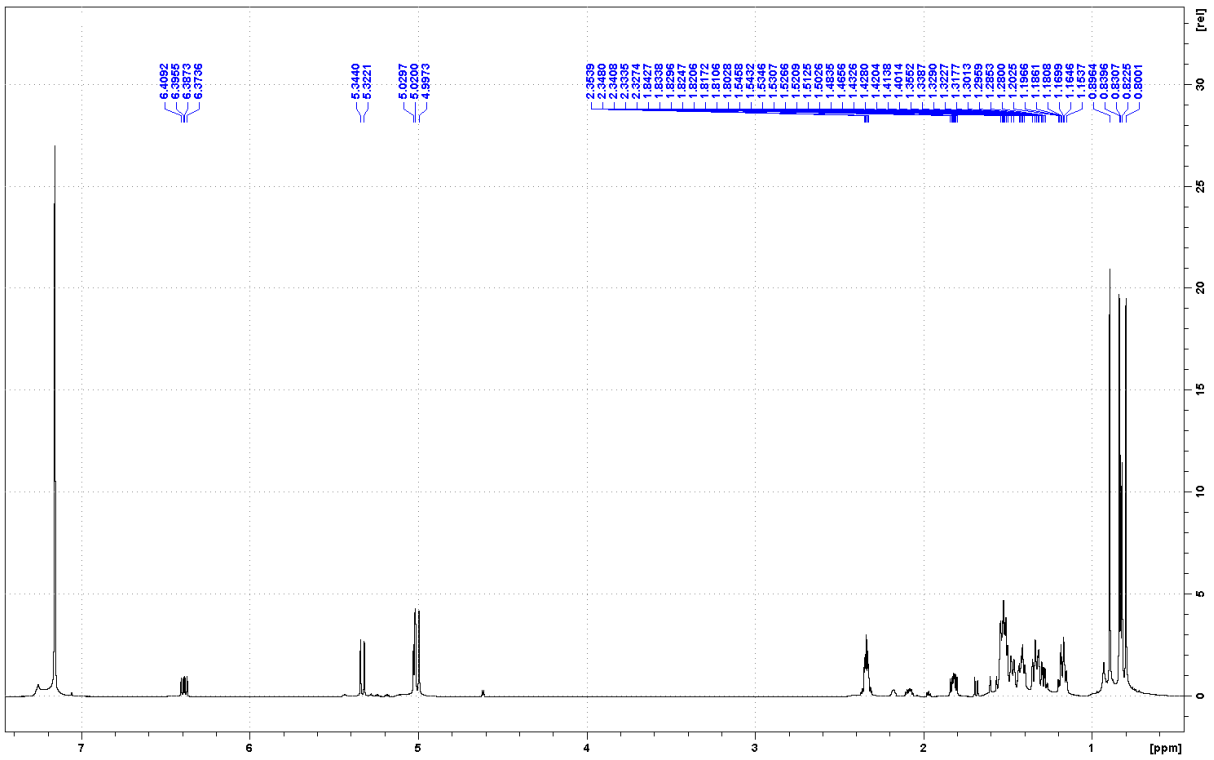

(B) ^{13}C Spectrum of (8*R*,9*R*,10*S*)-labda-13(16),14-dien-9-ol (**34**)

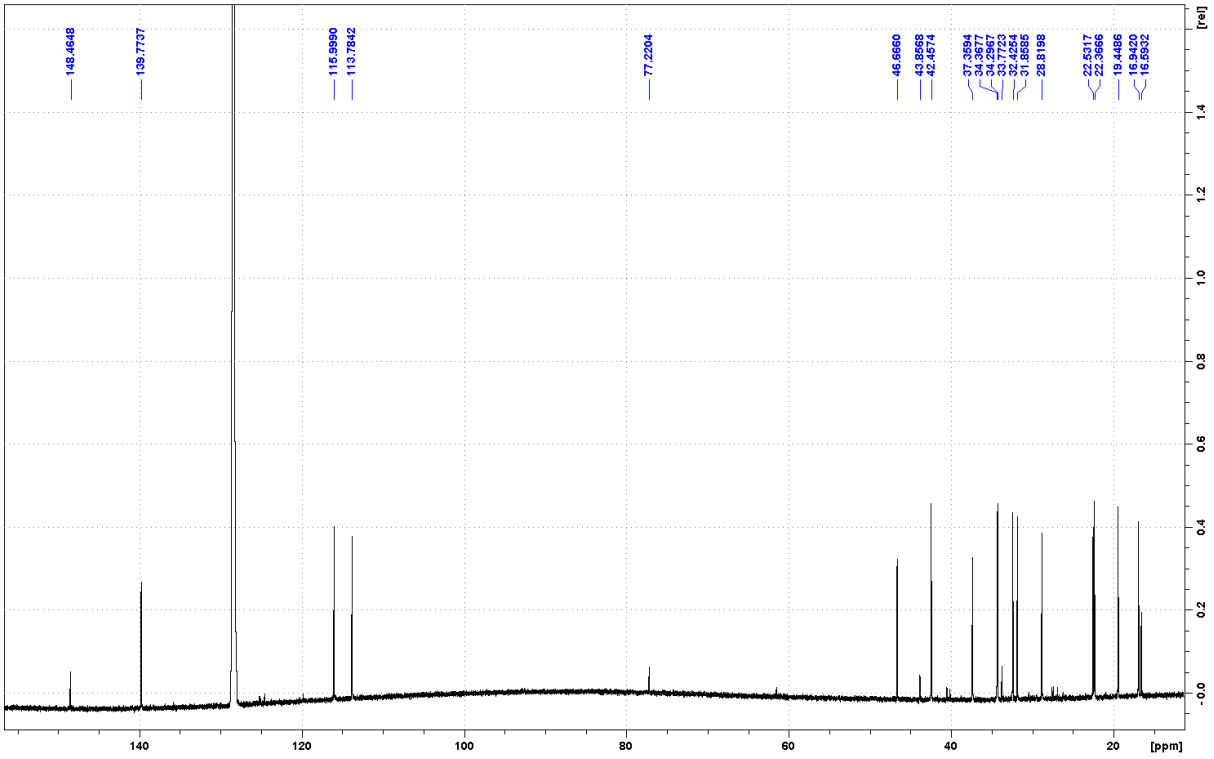

Fig. S19. Mass spectra for (A) **33**: viteagnusin D and (B) **34**: (8*R*,9*R*,10*S*)-labda-13(16),14-dien-9-ol.

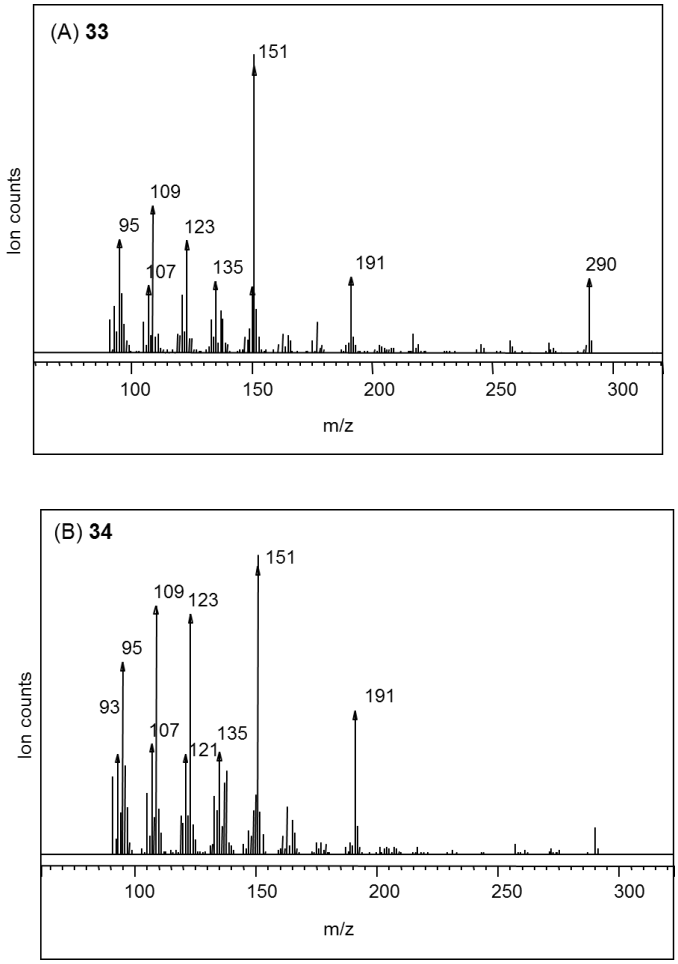

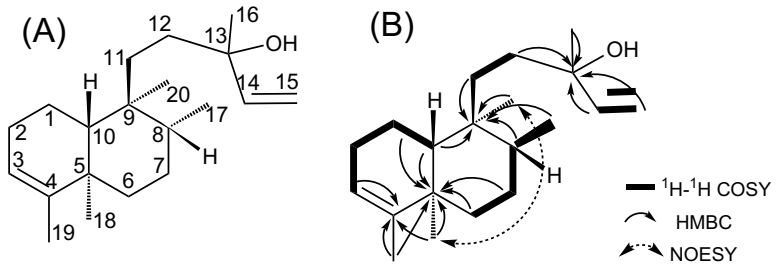

ent-kolavelool (**35**)

Fig. S20. The major product of SsSS co-expressed with AtCPS:H263Y. (A) Numbering; (B) ^{1}H-^{1}H COSY correlations, selected HMBC correlations and NOESY Nuclear Overhauser Effect dipole-dipole correlations used to assign the structure. The reported specific rotation of (13*R*)-*ent*-kolavelool was $[\alpha]_D^{25}$ =-40.4 (Nagashima et al., 2001) while we observed $[\alpha]_D^{25}$ =-20 for compound **35**. The difference between the numerical values of the specific rotation suggests that the configuration at C13 of **35** might be inferred to be *S*, but other analytical methods including X-ray crystallographic analysis of **35** would be required in order to establish the C13 stereochemistry without ambiguity.

Table S6: ^{1}H and ^{13}C NMR assignments for compound **35**, *ent*-kolavelool (solvent $CDCl_3$).

Position		*ent*-kolavelool (**35**)	
		δ_H	δ_C
1		1.39 (2H, m)	18.2
2	a	2.00 (1H, m)	27.1
	b	1.97 (1H, m)	
3		5.16 (1H, brs)	120.7
4			144.7
5			38.6
6	a	1.67 (1H, dt, *J* = 12.5, 3.5 Hz)	37.0
	b	1.14 (1H, td, *J* = 12.5, 4.3 Hz)	
7		1.38 (2H, m)	27.7
8		1.40 (1H, m)	36.4
9			38.4
10		1.28 (1H, m)	46.6
11		1.37 (2H, m)	32.1
12	a	1.36 (1H, m)	35.5
	b	1.33 (1H, m)	
13			73.7
14		5.86 (1H, dd, *J* = 17.2, 10.6 Hz)	145.4
15	a	5.18 (1H, d, *J* = 17.2 Hz)	112.0
	b	5.04 (1H, d, *J* = 10.6 Hz)	
16		1.25 (3H, s)	28.0
17		0.75 (3H, d, *J* = 6.1 Hz)	16.2
18		0.97 (3H, s)	20.1
19		1.56 (3H, q, *J* = 1.6 Hz)	18.4
20		0.70 (3H, s)	18.7

Fig. S21. (A) ^{1}H Spectrum of *ent*-kolavelool (**35**)

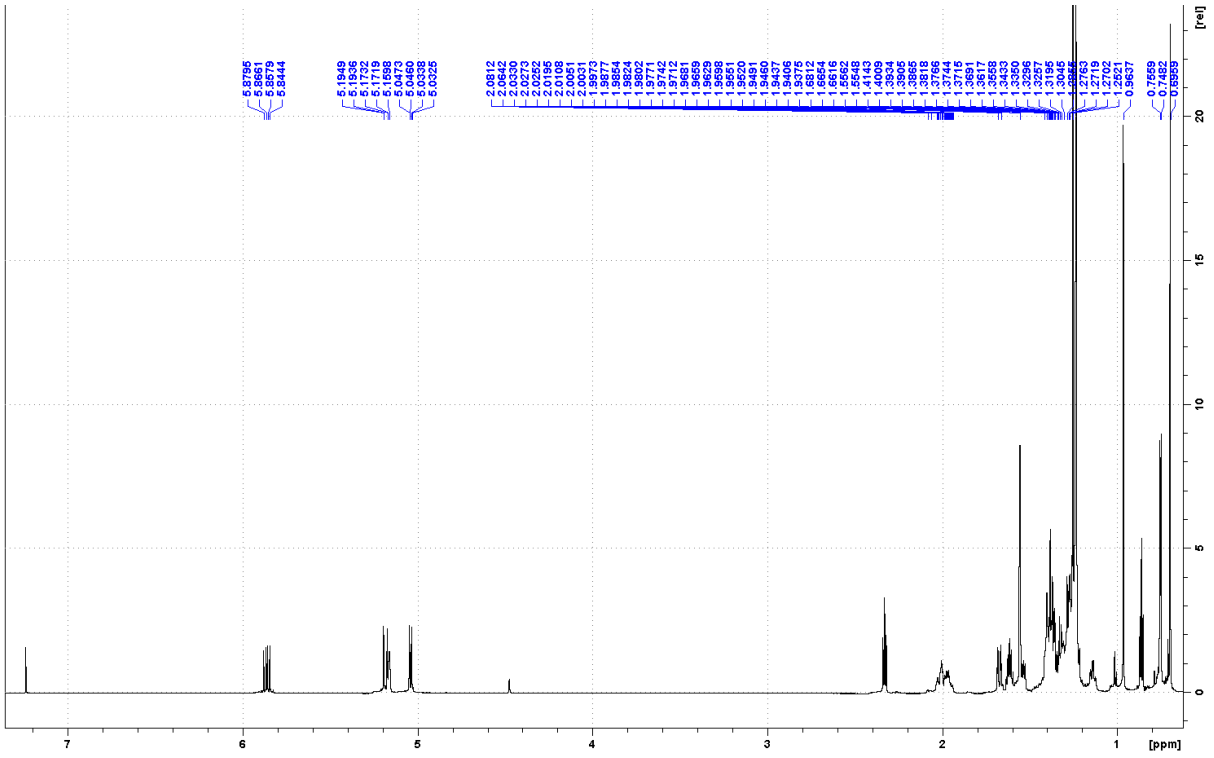

(B) ^{13}C Spectrum of *ent*-kolavelool (**35**)

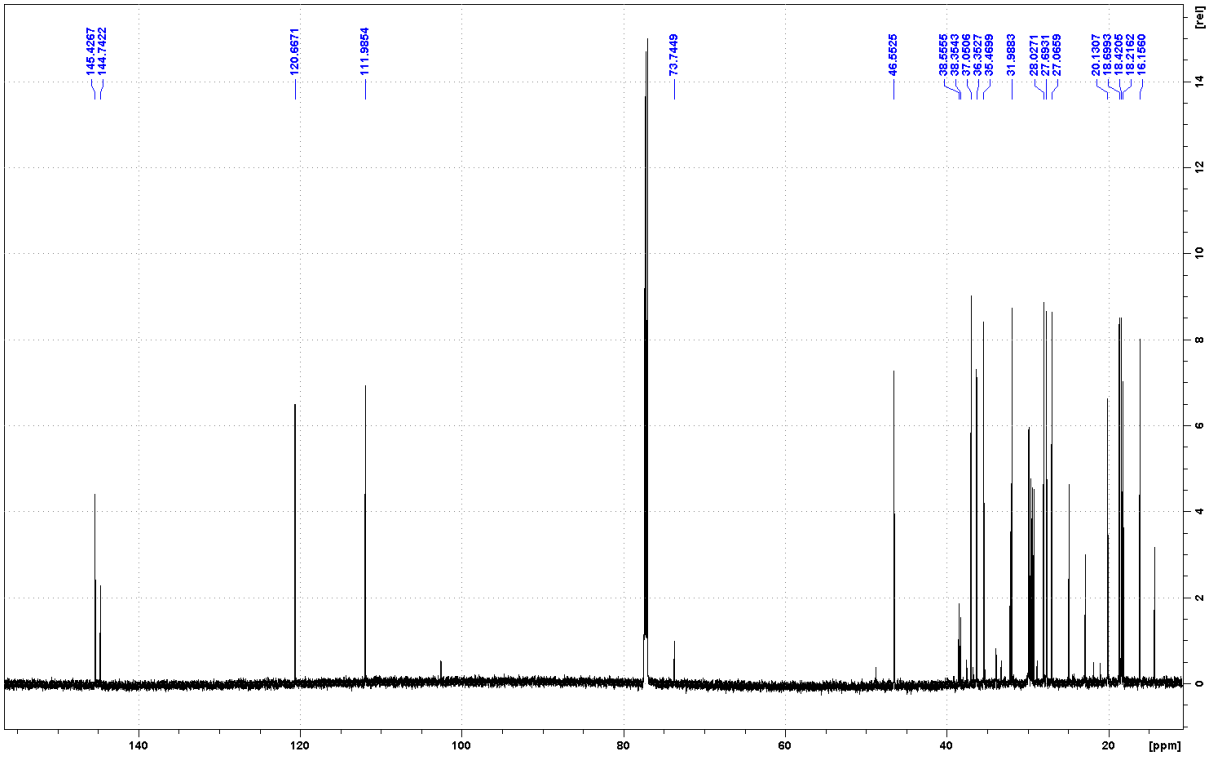

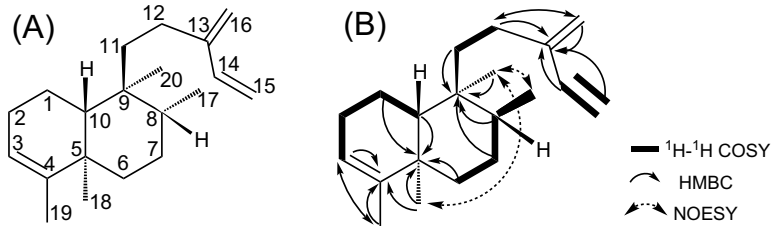

(5*R*,8*R*,9*S*,10*R*)-cleroda-3,13(16),14-triene (**36**)

Fig. S22. The major product of KgTS co-expressed with AtCPS:H263Y. (A) Numbering; (B) ^{1}H-^{1}H COSY correlations, selected HMBC correlations and NOESY Nuclear Overhauser Effect dipole-dipole correlations used to assign the structure.

Table S7: ^{1}H and ^{13}C NMR assignments for compound **36**, (5*R*,8*R*,9*S*,10*R*)-cleroda-3,13(16),14-triene (solvent $CDCl_3$).

Position		(5*R*,8*R*,9*S*,10*R*)-cleroda-3,13(16),14-triene (**36**)	
		δ_H	δ_C
1		1.41 (2H, m)	18.2
2		2.02 (2H, m)	27.1
3		5.17 (1H, brs)	120.7
4			144.8
5			38.5
6	a	1.69 (1H, dt, *J* = 12.8, 3.1 Hz)	37.0
	b	1.18 (1H, td, *J* = 12.8, 4.7 Hz)	
7		1.41 (2H, m)	27.8
8		1.53 (1H, m)	36.5
9			39.4
10		1.41 (1H, m)	46.7
11		1.41 (2H, m)	37.8
12	a	2.07 (1H, m)	24.9
	b	1.98 (1H, m)	
13			147.8
14		5.86 (1H, dd, *J* = 17.2, 10.6 Hz)	139.3
15	a	5.19 (1H, d, *J* = 17.6 Hz)	113.2
	b	5.02 (1H, d, *J* = 10.7 Hz)	
16		4.95 (2H, brs)	115.7
17		0.79 (3H, d, *J* = 7.0 Hz)	16.3
18		0.98 (3H, s)	20.2
19		1.57 (3H, q, *J* = 1.8 Hz)	18.5
20		0.69 (3H, s)	18.6

Fig. S23. (A) ^{1}H Spectrum of (5*R*,8*R*,9*S*,10*R*)-cleroda-3,13(16),14-triene (**36**)

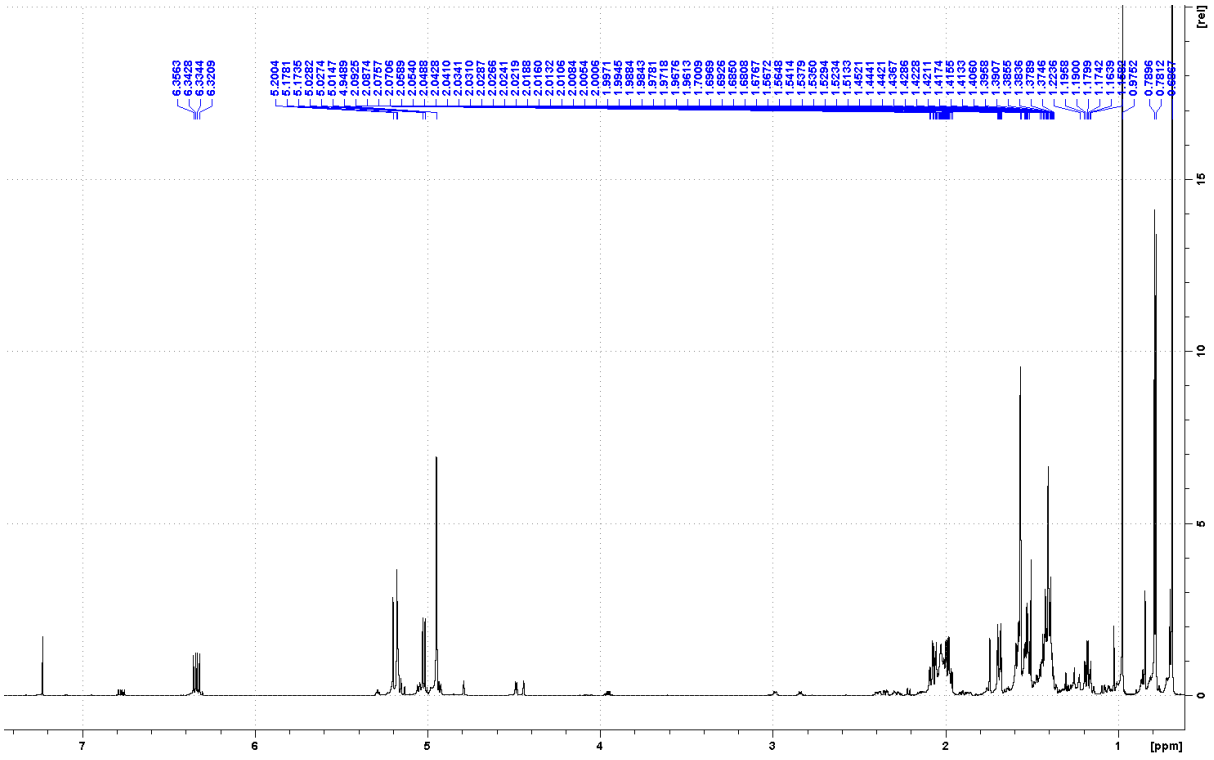

(B) ^{13}C Spectrum of (5*R*,8*R*,9*S*,10*R*)-cleroda-3,13(16),14-triene (**36**)

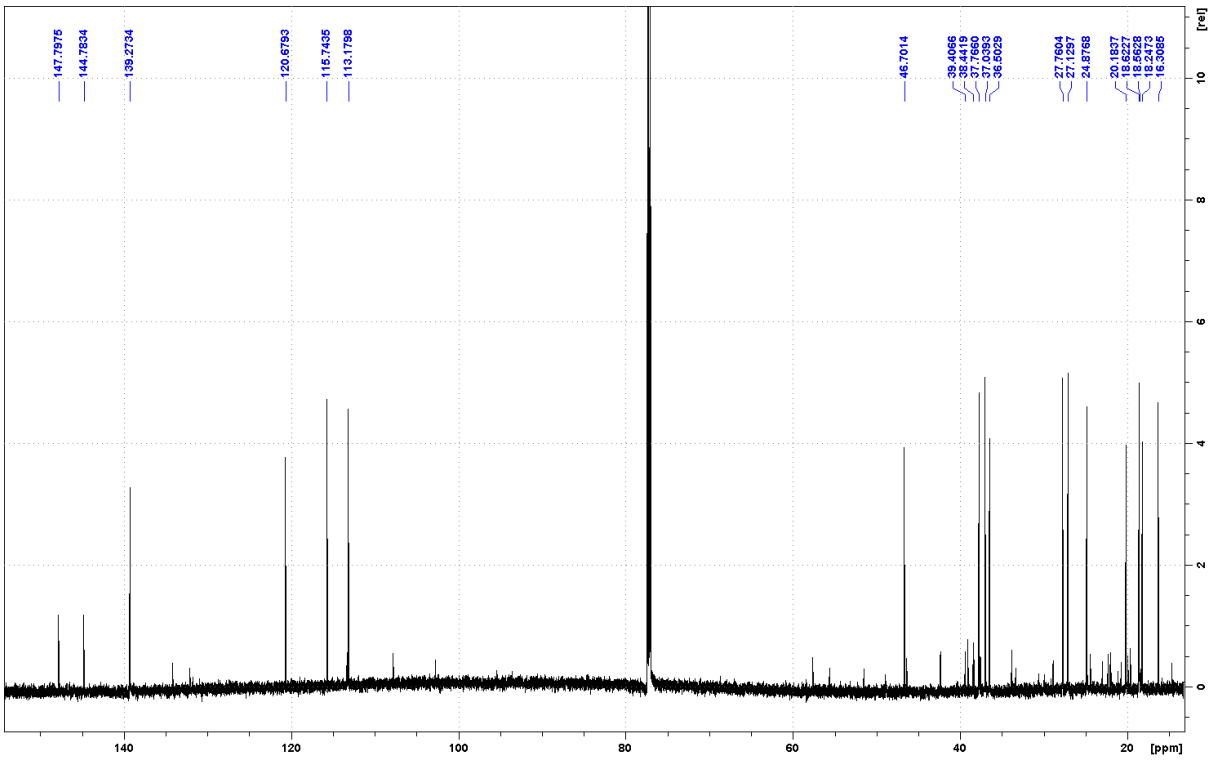

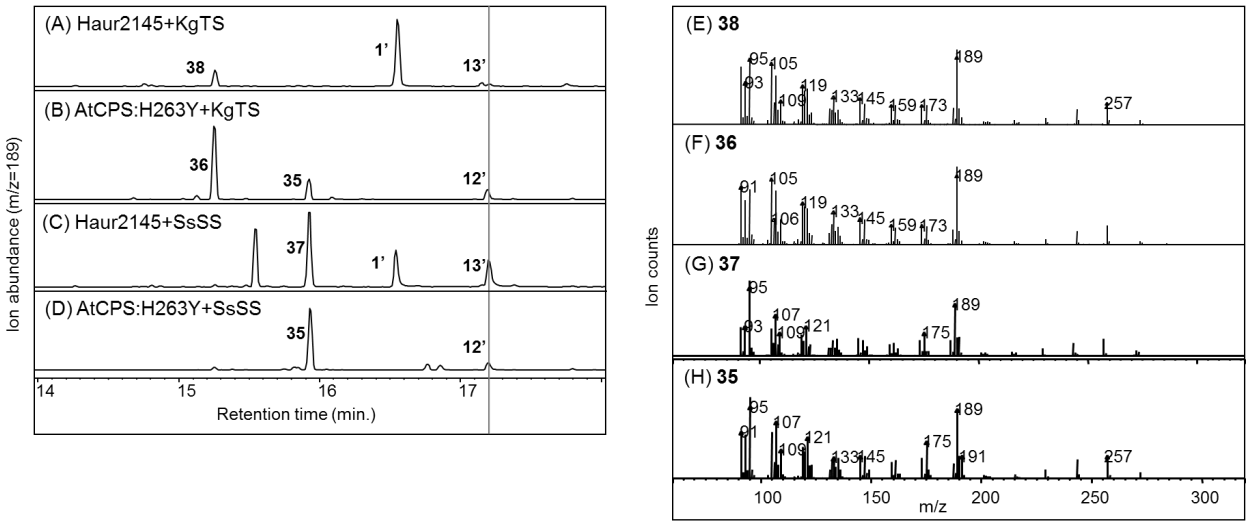

Fig. S24. Chromatograms from GC-MS analysis of extracts from *E. coli* engineered for production of kolavenyl diphosphate (**13**) by co-expressing Haur2145 with KgTS (A) or SsSS (C), or for production of *ent*-kolavenyl diphosphate (**12**) by co-expressing AtCPS:H263Y with KgTS (B) or SsSS (D) (numbering as defined in the text, with **13'** and **12'** corresponding to the dephosphorylated derivatives of **13** and **12**, respectively). Mass spectra for indicated peaks (E) **38**: (5*S*,8*S*,9*R*,10*S*)-cleroda-3,13(16),14-triene; (F) **36**: (5*R*,8*R*,9*S*,10*R*)-cleroda-3,13(16),14-triene; (G) **37**: kolavelool; (H) **35**: *ent*-kolavelool. Enzymatic products of KgTS and SsSS with **13** were identified by comparison (both retention time and mass spectra) to their respective enantiomers.

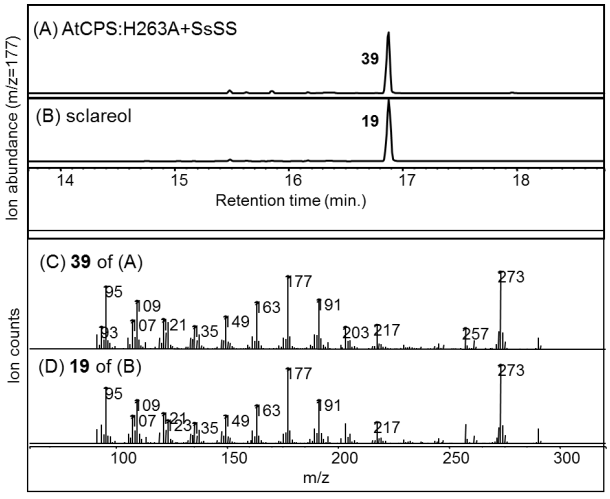

Fig. S25. Chromatograms from GC-MS analysis of extracts from *E. coli* engineered for production of 8β-hydroxy-*ent*-CPP (**8**) by co-expressing AtCPS:H263A with SsSS (A) (numbering as defined in the text, with **8'** corresponding to the dephosphorylated derivative of **8**). Mass spectra for indicated peaks (C) **39**: *ent*-sclareol; (D) **19**: sclareol standard. Enzymatic product of SsSS was identified by comparison (both retention time and mass spectra) to an authentic sclareol standard (B) (Aldrich).

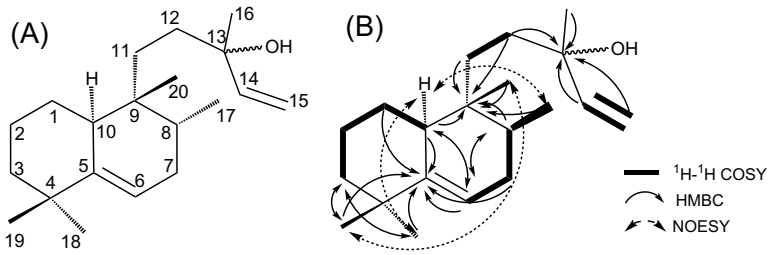

(8*R*,9*R*,10*S*)-halimada-5,14-dien-13-ol (**40**)

Fig. S26. The product of SsSS co-expressed with OsCPS4:H561D. (A) Numbering; (B) ^{1}H-^{1}H COSY correlations, selected HMBC correlations and NOESY Nuclear Overhauser Effect dipole-dipole correlations used to assign the structure. Note: As similarly reported for tuberculosinyl diphosphate (**10**) (Nakano et al., 2005), there are several exchangeable carbons and protons in compound **40**, resulting in lower resolution characterized by broad peaks. Therefore, a higher temperature condition (50 °C) for NMR measurement was used for compound **40** to obtain sharper peaks. Two split protons and corresponding carbons instead of one have been observed for H14, C14, H15 and C15 (Fig S25), which was suspected to be due to a racemic mixture of C13 isomers.

Table S8: ^{1}H and ^{13}C NMR assignments for compound **40**, (8*R*,9*R*,10*S*)-halimada-5,14-dien-13-ol (solvent $CDCl_3$).

Position		(8*R*,9*R*,10*S*)-halimada-5,14-dien-13-ol	
		δ_H	δ_C
1	a	1.73 (1H, m)	29.0
	b	1.03 (1H, m)	
2		1.58 (2H, m)	23.2
3	a	1.40 (1H, m)	42.3
	b	1.16 (1H, m)	
4			36.9
5			146.9
6		5.3 (1H, t, *J* = 3.6 Hz)	114.7
7	a	2.04 (1H, d, *J* = 13.0 Hz)	31.2
	b	1.66 (1H, m)	
8		1.59 (1H, m)	33.2
9			36.4
10		1.93 (1H, d, *J* = 12.5 Hz)	41.2
11	a	1.32 (1H, m)	35.9
	b	1.16 (1H, m)	
12	a	1.45 (1H, m)	35.9
	b	1.42 (1H, m)	
13			73.7
14		5.88 (1H, dd, *J* = 17.2, 10.6 Hz)	145.7
15	a	5.17 (1H, d, *J* = 17.2 Hz)	111.8
	b	5.00 (1H, d, *J* = 10.6 Hz)	
16		1.24 (3H, s)	27.9
17		0.75 (3H,d, *J* = 6.8 Hz)	14.8
18		0.99 (3H, s)	27.2
19		1.02 (3H, s)	29.7
20		0.77 (3H, s)	22.3

Fig. S27. (A) ^{1}H Spectrum of (8*R*,9*R*,10*S*)-halimada-5,14-dien-13-ol (**40**)

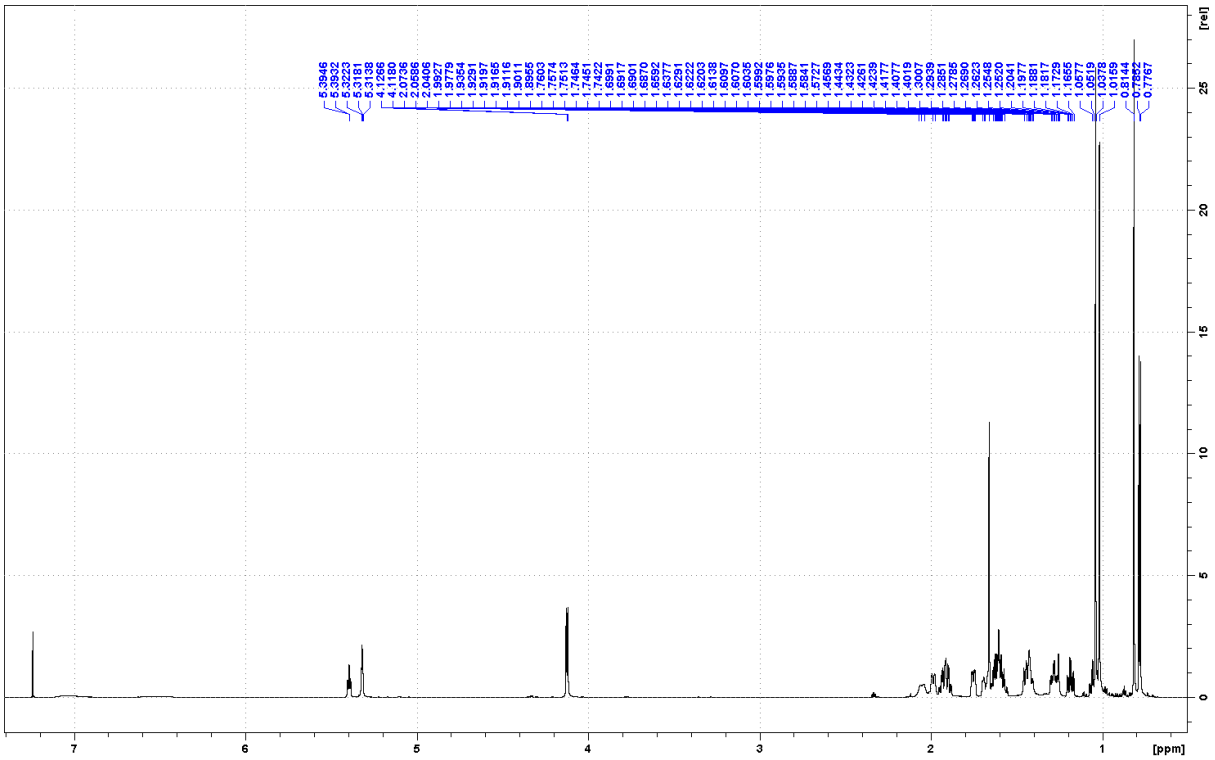

(B)^{13}C Spectrum of (8*R*,9*R*,10*S*)-halimada-5,14-dien-13-ol (**40**)

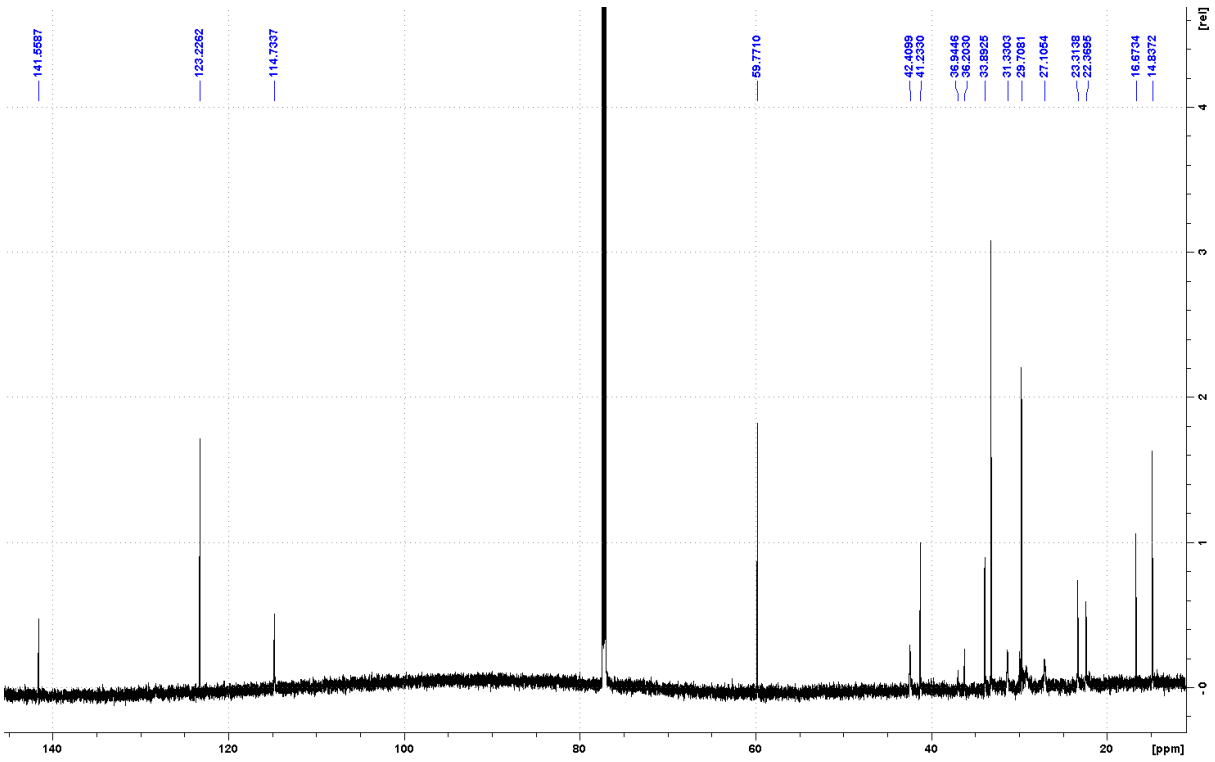

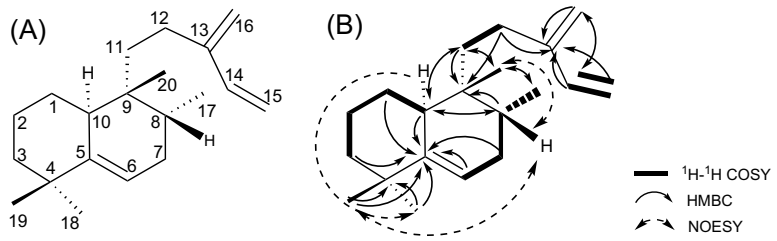

(8*R*,9*R*,10*S*)-halimada-5,13(16),14-triene (**41**)

Fig. S28. The product of KgTS co-expressed with OsCPS4:H561D. (A) Numbering; (B) ^{1}H-^{1}H COSY correlations, selected HMBC correlations and NOESY Nuclear Overhauser Effect dipole-dipole correlations used to assign the structure. Note: Similar to compound **40**, the NMR measurement was conducted at 50 °C to obtain sharper peaks.

Table S9: ^{1}H and ^{13}C NMR assignments for compound **41**, (8*R*,9*R*,10*S*)-halimada-5,13(16),14-triene (solvent $CDCl_3$).

Position		(8*R*,9*R*,10*S*)-halimada-5,13(16),14-triene	
		δ_H	δ_C
1	a	1.77 (1H, m)	29.1
	b	1.06 (1H, m)	
2		1.6 (2H, m)	23.3
3	a	1.44 (1H, td, *J* = 12.8, 5.4 Hz)	42.4
	b	1.19 (1H, m)	
4			36.9
5			146.9
6		5.33 (1H, t, *J* = 3.8 Hz)	114.8
7	a	2.07 (1H, d, *J* = 16.8 Hz)	31.3
	b	1.69 (1H, m)	
8		1.66 (1H, m)	33.2
9			36.5
10		2.02 (1H, d, *J* = 12.9 Hz)	41.2
11	a	1.52 (1H, m)	33.7
	b	1.36 (1H, m)	
12		2.13 (2H, m)	25.9
13			148.2
14		6.34 (1H, dd, *J* = 17.4, 10.7 Hz)	139.3
15	a	5.22 (1H, d, *J* = 17.4 Hz)	113.2
	b	5.02 (1H, d, *J* = 10.7 Hz)	
16		4.96 (2H, d, *J* = 5.4 Hz)	115.4
17		0.79 (3H,d, *J* = 6.7 Hz)	14.9
18		1.02 (3H, s)	27.2
19		1.05 (3H, s)	29.8
20		0.87 (3H, s)	22.4

Fig. S29. (A) ^{1}H Spectrum of (8*R*,9*R*,10*S*)-halimada-5,13(16),14-triene (**41**)

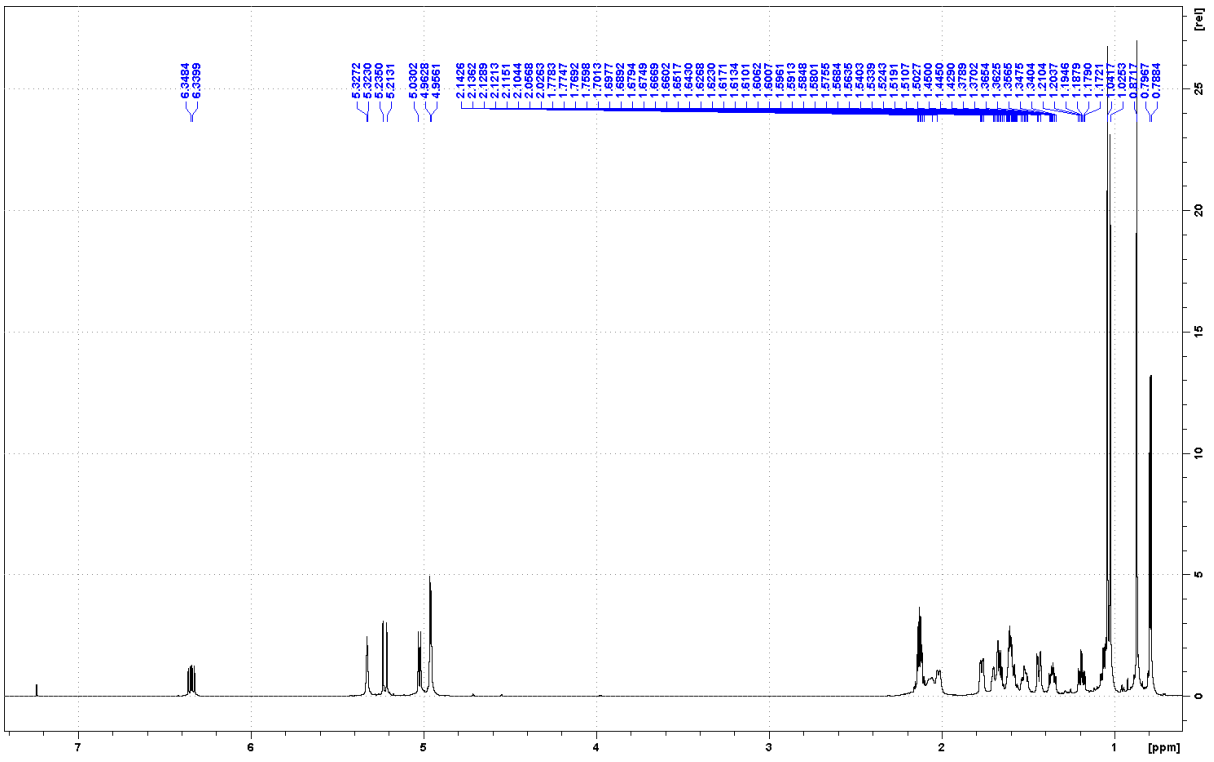

(B) ^{13}C Spectrum of (8*R*,9*R*,10*S*)-halimada-5,13(16),14-triene (**41**)

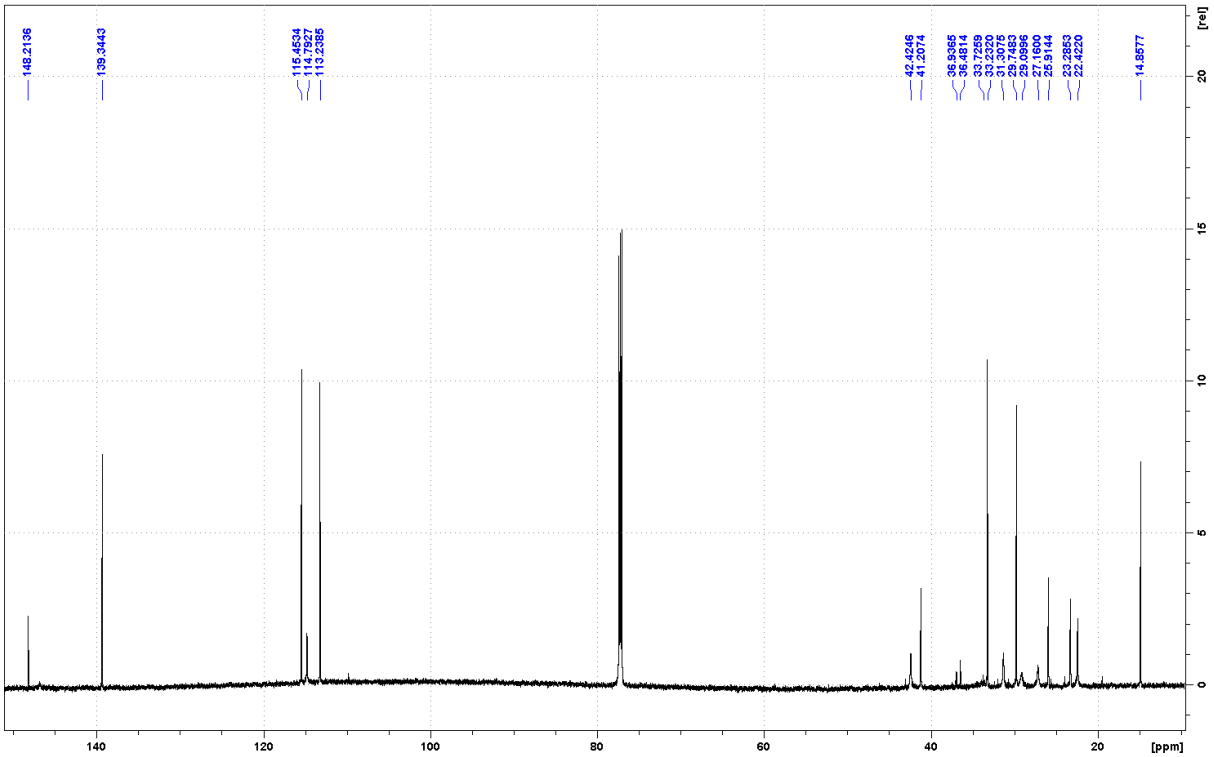

Fig. S30. Mass spectra for (A) **40**: (8*R*,9*R*,10*S*)-halimada-5,14-dien-13-ol and (B) **41**: (8*R*,9*R*,10*S*)-halimada-5,13(16),14-triene.

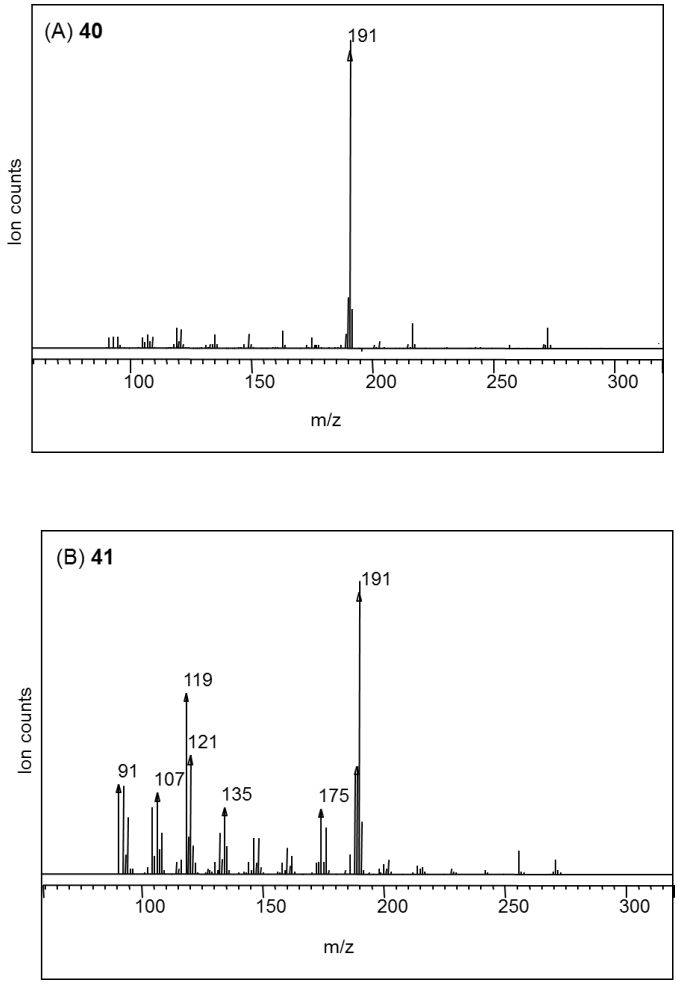

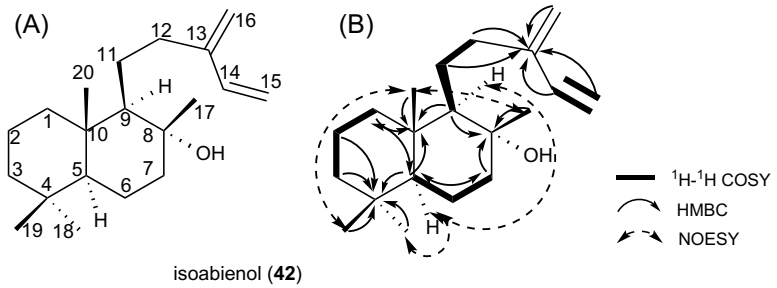

Fig. S31. The major product of KgTS co-expressed with NgCLS. (A) Numbering; (B) ^{1}H-^{1}H COSY correlations, selected HMBC correlations and NOESY Nuclear Overhauser Effect dipole-dipole correlations used to assign the structure. Note: Structural characterization of isoabienol has been previously reported (Cheng et al., 2012).

Table S10: ^{1}H and ^{13}C NMR assignments for compound **42**, isoabienol (solvent $CDCl_3$).

Position		isoabienol	
		δ_H	δ_C
1	a	0.98 (1H, td, *J* = 12.3, 3.2 Hz)	39.9
	b	1.65 (1H, m)	
2	a	1.57 (1H, m)	18.7
	b	1.41 (1H, m)	
3	a	1.35 (1H, d, *J* = 13.7 Hz)	42.2
	b	1.13 (1H, m)	
4			33.5
5		0.92 (1H, dd, *J* = 12.4, 2.0 Hz)	56.4
6	a	1.63 (1H, m)	20.8
	b	1.24 (1H, m)	
7	a	1.85 (1H, m)	44.8
	b	1.39 (1H, m)	
8			74.5
9		1.10 (1H, dd, *J* = 3.6, 3.6 Hz)	62.0
10			39.4
11	a	1.59 (1H, m)	24.8
	b	1.42 (1H, m)	
12	a	2.32 (1H, m)	35.3
	b	2.25 (1H, m)	
13			147.7
14		6.34 (1H, dd, *J* = 17.3, 10.9 Hz)	139.0
15	a	5.28 (1H, d, *J* = 17.3 Hz)	113.7
	b	5.04 (1H, d, *J* = 10.9 Hz)	
16		4.99 (2H, d, *J* = 8.0 Hz)	115.8
17		1.13 (3H, s)	24.2
18		0.77 (3H, s)	21.7
19		0.86 (3H, s)	33.6
20		0.77 (3H, s)	15.8

Fig. S32. (A) ^{1}H Spectrum of isoabienol (**42**)

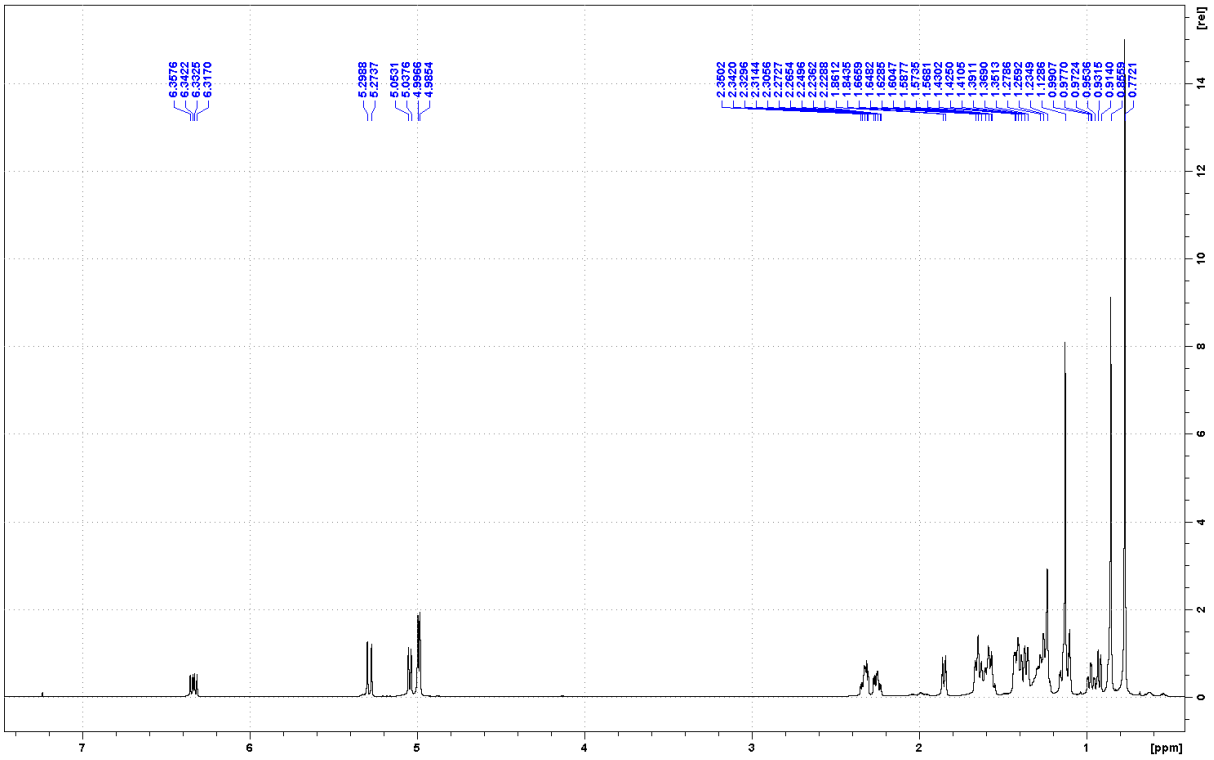

(B) ^{13}C Spectrum of isoabienol (**42**)

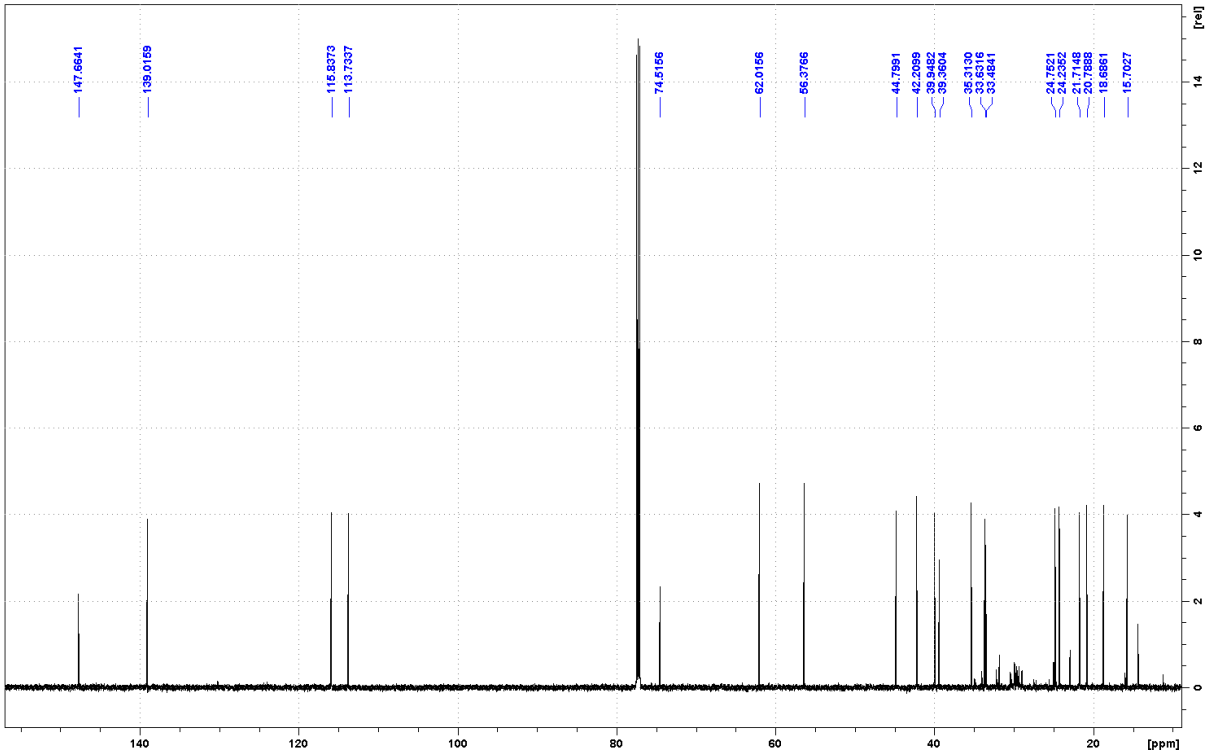

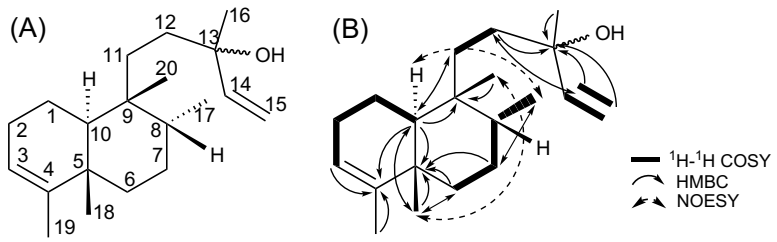

(5*S*,8*R*,9*R*,10*S*)-cleroda-3,14-dien-13-ol (**43**)

Fig. S33. The product of SsSS co-expressed with KgTPS. (A) Numbering; (B) ^{1}H-^{1}H COSY correlations, selected HMBC correlations and NOESY Nuclear Overhauser Effect dipole-dipole correlations used to assign the structure. From its original 1D ^{1}H and ^{13}C spectra (Fig S31), two split protons and corresponding carbons instead of one have been observed for H14, C14, H15 and C15 (Fig S25), which was suspected to be due to a racemic mixture of C13 isomers.

Table S11: ^{1}H and ^{13}C NMR assignments for compound **43**, (5*S*,8*R*,9*R*,10*S*)-cleroda-3,14-dien-13-ol (solvent $CDCl_3$).

Position		(5*S*,8*R*,9*R*,10*S*)-cleroda-3,14-dien-13-ol	
		δ_H	δ_C
1	a	1.61 (1H, m)	18.0
	b	1.38 (1H, m)	
2	a	2.03 (1H, m)	27.0
	b	1.97 (1H, m)	
3		5.13 (1H, brs)	120.4
4			144.8
5			38.5
6		1.41 (2H, m)	30.4
7	a	1.90 (1H, tt, *J* = 13.8, 4.4 Hz)	25.8
	b	1.24 (1H, m)	
8		1.53 (1H, m)	35.4
9			37.4
10		1.39 (1H, m)	45.4
11	a	1.42 (1H, m)	33.0
	b	0.99 (1H, m)	
12		1.47 (2H, m)	35.3
13			73.8
14		5.89 (1H, dd, *J* = 17.3, 10.7 Hz)	145.5
15	a	5.18 (1H, d, *J* = 17.3 Hz)	111.9
	b	5.03 (1H, d, *J* = 10.8 Hz)	
16		1.27 (3H, s)	28.0
17		0.88 (3H, d, *J* = 7.3 Hz)	15.0
18		1.02 (3H, s)	20.8
19		1.56 (3H, q, *J* = 1.8 Hz)	18.2
20		0.87 (3H, s)	20.6

Fig. S34. (A) ^{1}H Spectrum of (5*S*,8*R*,9*R*,10*S*)-cleroda-3,14-dien-13-ol (**43**)

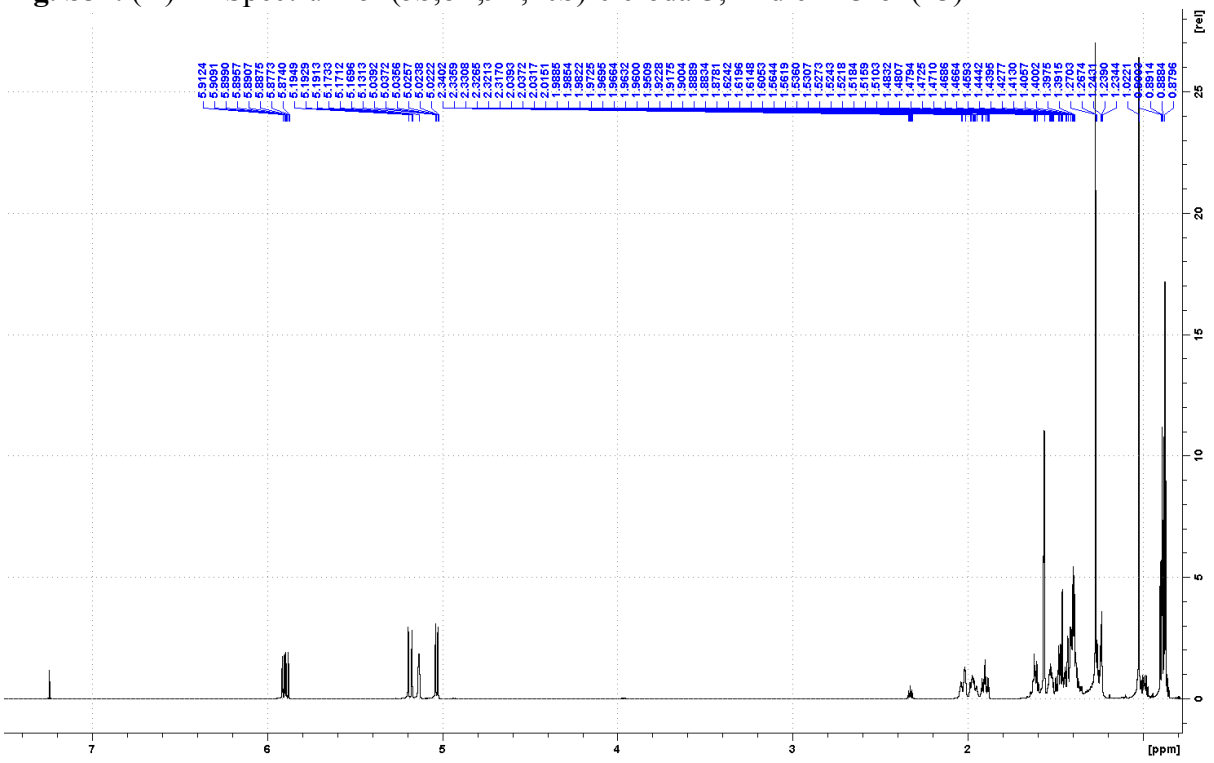

(B) ^{13}C Spectrum of (5*S*,8*R*,9*R*,10*S*)-cleroda-3,14-dien-13-ol (**43**)

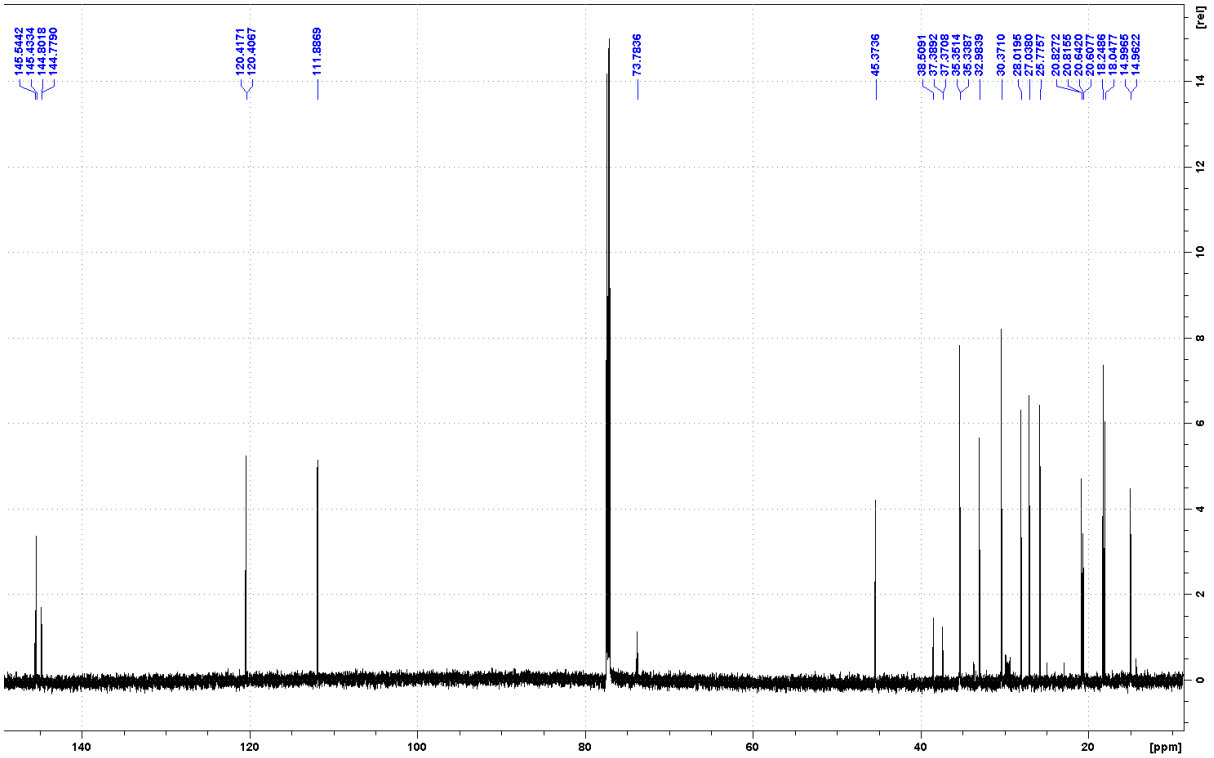

Fig. S35. Mass spectra for (A) **42**: *iso*-abienol and (B) **43**: (5*S*,8*R*,9*R*,10*S*)-cleroda-3,14-dien-13-ol.

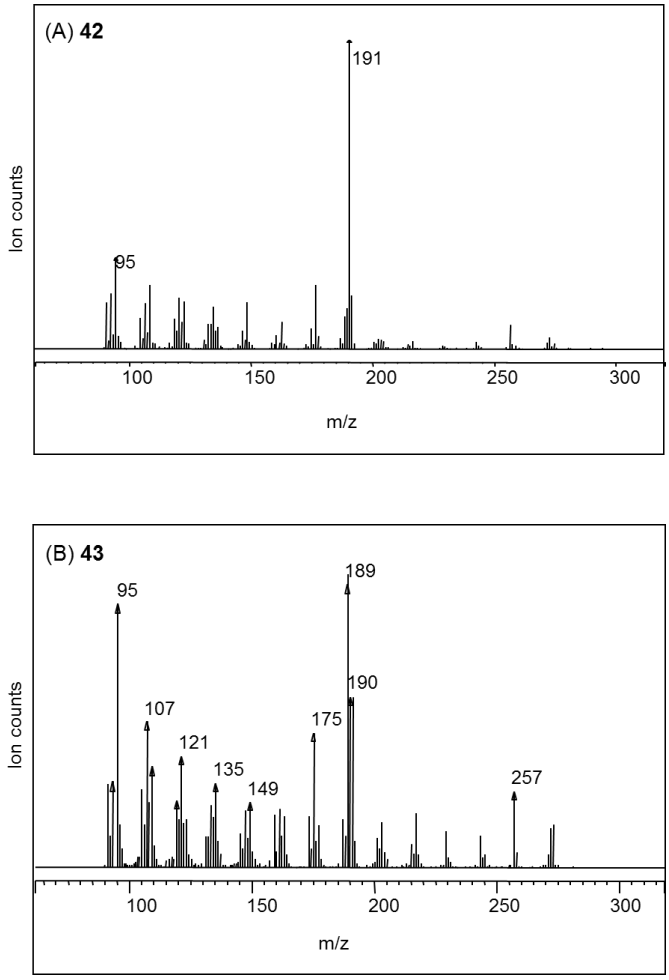

Synthetic gene sequences

SsSS Δ50 (the N-terminal transit peptide sequence was not included)

ATGGCAAAAATGAAAGAAAACTTTAAACGCGAAGATGACAAATTCCCGACCACCACCACGCTGCGCTCAGAAGAT
ATTCCGTCCAATCTGTGCATTATCGATACCCTGCAGCGTCTGGGCGTGGACCAGTTTTTCCAATACGAAATCAAC
ACCATCCTGGATAACACGTTTCGCCTGTGGCAAGAAAAACATAAAGTGATCTACGGTAACGTTACCACGCACGCA
ATGGCTTTCCGTCTGCTGCGCGTCAAAGGCTATGAAGTGAGCTCTGAAGAACTGGCACCGTACGGTAACCAGGAA
GCTGTTAGCCAGCAAACCAATGATCTGCCGATGATTATCGAACTGTATCGTGCGGCCAATGAACGCATTTACGAA
GAAGAACGTTCGCTGGAAAAAATTCTGGCGTGGACCACGATCTTTCTGAACAAACAGGTCCAAGATAATTCAATC
CCGGACAAAAAACTGCATAAACTGGTGGAATTTTACCTGCGTAACTACAAAGGCATTACGATCCGCCTGGGTGCA
CGTCGCAATCTGGAACTGTATGATATGACCTATTACCAGGCTCTGAAATCTACGAACCGCTTTAGTAACCTGTGC
AATGAAGACTTTCTGGTGTTCGCGAAACAGGATTTCGACATTCACGAAGCCCAGAATCAAAAAGGCCTGCAGCAA
CTGCAACGTTGGTACGCGGATTGTCGCCTGGACACCCTGAACTTTGGCCGTGATGTGGTTATTATCGCAAATTAT
CTGGCTTCCCTGATTATCGGTGATCATGCCTTTGACTACGTTCGCCTGGCGTTCGCCAAAACCTCAGTCCTGGTG
ACGATTATGGATGACTTTTTCGATTGCCACGGCAGTTCCCAGGAATGTGACAAAATCATCGAACTGGTTAAAGAA
TGGAAAGAAAACCCGGATGCGGAATATGGTAGCGAAGAACTGGAAATCCTGTTTATGGCCCTGTACAACACCGTC
AATGAACTGGCAGAACGTGCCCGCGTTGAACAGGGTCGTTCTGTCAAAGAATTTCTGGTCAAACTGTGGGTGGAA
ATTCTGAGTGCATTCAAAATCGAACTGGATACCTGGTCCAACGGTACGCAGCAATCATTTGACGAATATATTTCA
TCGAGCTGGCTGTCGAATGGCAGCCGCCTGACCGGTCTGCTGACGATGCAGTTCGTTGGCGTCAAACTGTCGGAT
GAAATGCTGATGAGCGAAGAATGCACCGACCTGGCCCGTCATGTGTGTATGGTTGGTCGCCTGCTGAACGATGTG
TGCTCTAGTGAACGTGAACGCGAAGAAAATATTGCAGGCAAATCCTATTCAATCCTGCTGGCTACGGAAAAAGAT
GGTCGTAAAGTGTCTGAAGACGAAGCAATCGCTGAAATCAACGAAATGGTTGAATATCACTGGCGCAAAGTTCTG
CAGATTGTCTACAAAAAAGAAAGTATCCTGCCGCGTCGCTGTAAAGATGTTTTTCTGGAAATGGCGAAAGGCACC
TTCTATGCCTACGGTATCAATGATGAACTGACCTCGCCGCAGCAATCGAAAGAAGACATGAAATCGTTTGTGTTT
TAA

Haur_2145 (full length)

ATGAGCCTGATTGTGGATATCCTGATTGATGATCTGCGTGCACTGATTCGTGATCTGGGTCAGAATGGTGGTCTG
ATGAGCCCGAGCGTTTATGATACCAGCCAGGCACTGCGTCTGTATCCGACCCCGAGCGAAGAACATGTTTGGCCT
GCAGTTAATTGGCTGATTAGCCAGCAGCAGAGTGATGGTGGTTGGGGTAATCCGAGCATGCCGCTGAGCCGTGCA
GTTCCGACCCTGGCAGCAATTCTGGCCCTGCGTCGTCATTGTCAGCGTCGTAGCACCTTTGATGGTCTGCTGGAA
GCCAAACGTTTTCTGCGTCGCCAGCTGGAATATTGGGAAAAACCGCTGCCGGATAATCTGCCGGTTGGTATGGAA
CTGCTGCTGCCGTATATGCTGGAAGAAGCATATCGGGAAGAACATCAGGATGATATTGATGATGTTCCGATTAAA
CTGCGCCTGAACATTCCGCTGGCACCGTATCGTGAACTGATTGCACTGGGTGAACATAAACGTAGCCTGATTCAG
CAGAAAAAACCGCGTGCAGGCACCGCACCGGTTTATAGCTGGGAAGCATGGGCAAGCCATGCAGATCCGGAACTG
ATCGATGGTAGCGGTGGTATTGGTCATAGTCCGGCAGCAACCGCAGCATGGCTGTTTGCAGCAAATCATAATCCG
AATCTGCGTAATGAAATTGCCGGTGCAGAAAATTATCTGCGTCAGGCAAGCCTGGCAACCAGCGAAAGCGCACCG
TGTATTATGCCGACCGCATGGCCGATTCCGCGTTTTGAACAGAGCTTTAGCCTGTATGCACTGGTTACCGGTGGC
ATTCTGGATTTTCCGAGCATTCAGGATGTTCTGAAACCGCAGATTGCCGATCTGCATCAGGCCCTGAAACCTCGC
GGTATTGGTTTTAGTGATGATTTTATGCCGGATGGTGATGATACCGCAGCAGCGGTTGCAGTTCTGATTGCAGCA
GGTTATCCGGTTGATCTGGCAATTCTGAATCAGTTTGAACGCGAACCGTATTTTGTTGCCTATCATGGTGAACTG
CAGCCGAGCATTAGCCTGACCGCACGTGCCGTTCATGCACTGGATCTGGCAGGCGTTGATATTAGCCGTTGGTGG
AAAATCTTTATCGATGCACAGAAACTGGATGGTAGCTGGTCAGGTGATAAATGGAATACCAGCTGGCTGTATACC
ACCTGTCATGTGCTGATTGCCCTGAAAAATAGCCCGTATAAAACCGCAATGAAAGAAGCAGTTGCAGCACTGCAG

GTTCATCAGCATCCAGATGGCGGATGGGGTATTATCAATCGTAGTACCACCGTTGAAACCGCCTATGCCGTTCTG
GCACTGCAGAATCTGCGCGAAGCTGGCCTGCTGGATGATGACGATATCCACATGCTGCAGCGTGGTTATAACTGG
CTGTGTATTCATTATCGTCCGTTCCGTATGAAAGAATATCAGTGCTGGCTGAACAAAGAGATTTATTGTCCGCAG
CGTATTGATCGTGCCTATGAACTGAGCGCAATGCTGGCAGTTACCCTGGGCGAACTGAAACTGTAA

MvCPS1 Δ15 (the N-terminal transit peptide sequence was not included)

ATGGTGCGTACCAAAATTCCGGCAAAAATTAGCCTGCCTGCATGTAGCTGGCTGGATCGTAGCAGCAGCCGTCAT
GTTGAACTGAATCACAAATTTTGCCGTAAACTGGAACTGAAAGTTGCAATGTGTCGTGCAAGCCTGGATGTTCAG
CAGGTTCGTGATGAAGTTTATAGCAATGCACAGCCGCATGAACTGGTTGACAAAAAAATCGAAGAACGCGTGAAA
TATGTGAAAAATCTGCTGAGCACAATGGATGATGGTCGTATTAATTGGAGCGCCTATGATACCGCATGGATTAGC
CTGATTAAAGATTTTGAAGGTCGTGATTGTCCGCAGTTTCCGAGCACCCTGGAACGTATTGCAGAAAATCAGCTG
CCGGATGGTAGCTGGGGTGATAAAGATTTCGATTGTAGCTATGATCGCATCATTAATACCCTGGCATGTGTTGTT
GCACTGACCACCTGGAATGTTCATCCGGAAATCAATCAGAAAGGTATCCGCTATCTGAAAGAAAACATGCGCAAA
CTGGAAGAAACCCCGACCGTTCTGATGACCTGTGCATTTGAAGTTGTTTTTCCGGCACTGCTGAAAAAAGCACGT
AATCTGGGTATTCATGATCTGCCGTATGATATGCCGATTGTGAAAGAAATTTGCAAAATCGGCGACGAAAAACTG
GCACGTATTCCGAAAAAAATGATGGAAAAAGAAACCACGAGCCTGATGTATGCAGCAGAAGGTGTTGAAAATCTG
GATTGGGAACGTCTGCTGAAACTGCGTACACCGGAAAATGGTAGCTTTCTGAGCAGTCCGGCAGCAACCGTTGTT
GCATTTATGCATACCAAAGATGAAGATTGCCTGCGCTATATCAAATATCTGCTGAATAAATTCAATGGTGGCGCA
CCGAATGTGTATCCGGTTGATCTGTGGTCACGTCTGTGGGCAACCGATCGTCTGCAGCGCCTGGGTATTAGCCGT
TATTTTGAAAGCGAAATTAAAGACCTGCTGAGCTATGTTCATAGCTATTGGACCGATATTGGTGTTTATTGTACC
CGTGATAGCAAATATGCGGATATTGATGATACCAGTATGGGTTTTCGTCTGCTGCGTGTTCAGGGCTATAATATG
GATGCCAATGTGTTCAAATATTTCCAGAAAGATGATAAATTTGTGTGCCTGGGTGGTCAGATGAATGGTAGCGCA
ACCGCAACCTATAATCTGTATCGTGCAGCACAGTATCAGTTTCCGGGTGAGCAGATTCTGGAAGATGCACGTAAA
TTTAGCCAGCAGTTTCTGCAAGAAAGCATCGATACCAATAACCTGCTGGATAAATGGGTTATTTCACCGCATATT
CCGGAAGAAATGCGTTTTGGTATGGAAATGACCTGGTATAGCTGTCTGCCTCGTATTGAAGCAAGCTATTATCTG
CAGCATTATGGTGCAACCGAAGATGTTTGGCTGGGTAAAACCTTTTTTCGCATGGAAGAAATCAGCAACGAAAAT
TATCGTGAACTGGCCATTCTGGACTTTAGCAAATGTCAGGCACAGCATCAGACCGAATGGATTCACATGCAAGAA
TGGTATGAAAGCAACAACGTGAAAGAGTTTGGCATTAGCCGTAAAGATCTGCTGTTTGCATATTTTCTGGCAGCA
GCAAGCATTTTTGAAACCGAACGTGCAAAAGAACGTATCCTGTGGGCACGTAGCAAAATCATTTGTAAAATGGTG
AAAAGCTTCCTGGAAAAAGAGACAGGTAGCCTGGAACATAAAATTGCATTTCTGACCGGTAGTGGCGATAAAGGT
AATGGTCCGGTTAATAATGCAATGGCAACCCTGCATCAGCTGCTGGGTGAATTTGATGGTTATATTAGCATTCAG
CTGGAAAATGCATGGGCAGCATGGCTGACCAAACTGGAACAGGGTGAAGCAAATGATGGTGAGCTGCTGGCAACC
ACCATTAACATTTGTGGTGGTCGTGTTAATCAGGATACCCTGAGCCATAATGAATATAAAGCACTGAGCGATCTG
ACCAACAAAATTTGCCATAATCTGGCGCAGATCCAGAATGATAAAGGTGATGAAATCAAAGACAGCAAACGTAGC
GAACGCGATAAAGAAGTTGAACAGGATATGCAGGCACTGGCAAAACTGGTTTTTGAAGAAAGCGATCTGGAACGC
AGCATTAAACAGACCTTTCTGGCCGTTGTTCGTACCTATTATTACGGTGCATATATCGCAGCCGAGAAAATTGAT
GTCCACATGTTTAAAGTGCTGTTTAAACCGGTGGGCTAA

References

Burke, C., Croteau, R., 2002. Interaction with the small subunit of geranyl diphosphate synthase modifies the chain length specificity of geranylgeranyl diphosphate synthase to produce geranyl diphosphate. J. Biol. Chem. 277**,** 3141-3149.

Cheng, S. S., Chung, M. J., Lin, C. Y., Wang, Y. N., Chang, S. T., 2012. Phytochemicals from Cunninghamia konishii Hayata act as antifungal agents. Journal of agricultural and food chemistry. 60**,** 124-8.

Criswell, J., Potter, K., Shephard, F., Beale, M. H., Peters, R. J., 2012. A single residue change leads to a hydroxylated product from the class II diterpene cyclization catalyzed by abietadiene synthase. Organic letters. 14**,** 5828-31.

Cyr, A., Wilderman, P. R., Determan, M., Peters, R. J., 2007. A modular approach for facile biosynthesis of labdane-related diterpenes. Journal of the American Chemical Society. 129**,** 6684-5.

Harris, L. J., Saparno, A., Johnston, A., Prisic, S., Xu, M., Allard, S., Kathiresan, A., Ouellet, T., Peters, R. J., 2005. The maize An2 gene is induced by Fusarium attack and encodes an ent-copalyl diphosphate synthase. Plant Mol Biol. 59**,** 881-894.

Herde, M., Gartner, K., Kollner, T. G., Fode, B., Boland, W., Gershenzon, J., Gatz, C., Tholl, D., 2008. Identification and regulation of TPS04/GES, an *Arabidopsis* geranyllinalool synthase catalyzing the first step in the formation of the insect-induced volatile C16-homoterpene TMTT. Plant Cell. 20**,** 1152-68.

Hoshino, T., Nakano, C., Ootsuka, T., Shinohara, Y., Hara, T., 2011. Substrate specificity of Rv3378c, an enzyme from Mycobacterium tuberculosis, and the inhibitory activity of the bicyclic diterpenoids against macrophage phagocytosis. Organic & biomolecular chemistry. 9**,** 2156-65.

Ignea, C., Ioannou, E., Georgantea, P., Loupassaki, S., Trikka, F. A., Kanellis, A. K., Makris, A. M., Roussis, V., Kampranis, S. C., 2015. Reconstructing the chemical diversity of labdane-type diterpene biosynthesis in yeast. Metabolic engineering. 28**,** 91-103.

Mafu, S., Hillwig, M. L., Peters, R. J., 2011. A novel labda-7,13e-dien-15-ol-producing bifunctional diterpene synthase from *Selaginella moellendorffii*. ChemBioChem. 12**,** 1984-7.

Mafu, S., Potter, K. C., Hillwig, M. L., Schulte, S., Criswell, J., Peters, R. J., 2015. Efficient heterocyclisation by (di)terpene synthases. Chemical communications.

Mann, F. M., Prisic, S., Hu, H., Xu, M., Coates, R. M., Peters, R. J., 2009. Characterization and inhibition of a class II diterpene cyclase from Mycobacterium tuberculosis: implications for tuberculosis. The Journal of biological chemistry. 284**,** 23574-9.

Matsuba, Y., Zi, J., Jones, A. D., Peters, R. J., Pichersky, E., 2015. Biosynthesis of the diterpenoid lycosantalonol via nerylneryl diphosphate in Solanum lycopersicum. PloS one. 10**,** e0119302.

Morrone, D., Lowry, L., Determan, M. K., Hershey, D. M., Xu, M., Peters, R. J., 2010. Increasing diterpene yield with a modular metabolic engineering system in E. coli: comparison of MEV and MEP isoprenoid precursor pathway engineering. Applied microbiology and biotechnology. 85**,** 1893-906.

Nagashima, F., Suzuki, M., Takaoka, S., Asakawa, Y., 2001. Sesqui- and diterpenoids from the Japanese liverwort Jungermannia infusca. Journal of natural products. 64**,** 1309-17.

Nakano, C., Hoshino, T., Sato, T., Toyomasu, T., Dairi, T., Sassa, T., 2010. Substrate specificity of the CYC2 enzyme from Kitasatospora griseola: production of sclarene, biformene, and novel bicyclic diterpenes by the enzymatic reactions of labdane- and halimane-type diterpene diphosphates. Tetrahedron Letters. 51**,** 125-128.

Nakano, C., Okamura, T., Sato, T., Dairi, T., Hoshino, T., 2005. Mycobacterium tuberculosis H37Rv3377c encodes the diterpene cyclase for producing the halimane skeleton. Chemical communications. 1016-1018.

Nakano, C., Oshima, M., Kurashima, N., Hoshino, T., 2015. Identification of a new diterpene biosynthetic gene

cluster that produces O-methylkolavelool in Herpetosiphon aurantiacus. Chembiochem : a European journal of chemical biology. 16**,** 772-81.

Ono, M., Yamasaki, T., Konoshita, M., Ikeda, T., Okawa, M., Kinjo, J., Yoshimitsu, H., Nohara, T., 2008. Five new diterpenoids, viteagnusins A--E, from the fruit of Vitex agnus-castus. Chem Pharm Bull (Tokyo). 56**,** 1621-4.

Peters, R. J., Ravn, M. M., Coates, R. M., Croteau, R. B., 2001. Bifunctional abietadiene synthase: Free diffusive transfer of the (+)-copalyl diphosphate intermediate between two distinct active sites. J. Am. Chem. Soc. 123**,** 8974-8978.

Potter, K., Criswell, J., Zi, J., Stubbs, A., Peters, R. J., 2014. Novel product chemistry from mechanistic analysis of ent-copalyl diphosphate synthases from plant hormone biosynthesis. Angewandte Chemie. 53**,** 7198-202.

Potter, K. C., Jia, M., Hong, Y. J., Tantillo, D. J., Peters, R. J., 2016a. Product rearrangement from altering a single residue in the rice syn-copalyl diphosphate synthase. Org. Lett. 18**,** 1060-1063.

Potter, K. C., Zi, J., Hong, Y. J., Schulte, S., Malchow, B., Tantillo, D. J., Peters, R. J., 2016b. Blocking Deprotonation with Retention of Aromaticity in a Plant ent-Copalyl Diphosphate Synthase Leads to Product Rearrangement. Angew. Chem. Int. Ed. 55**,** 634-638.

Xu, M., Hillwig, M. L., Prisic, S., Coates, R. M., Peters, R. J., 2004. Functional identification of rice *syn*-copalyl diphosphate synthase and its role in initiating biosynthesis of diterpenoid phytoalexin/allelopathic natural products. Plant J. 39**,** 309-318.

Zerbe, P., Chiang, A., Dullat, H., O'Neil-Johnson, M., Starks, C., Hamberger, B., Bohlmann, J., 2014. Diterpene synthases of the biosynthetic system of medicinally active diterpenoids in Marrubium vulgare. Plant J. 79**,** 914-27.

Zerbe, P., Chiang, A., Yuen, M., Hamberger, B., Hamberger, B., Draper, J. A., Britton, R., Bohlmann, J., 2012. Bifunctional cis-abienol synthase from Abies balsamea discovered by transcriptome sequencing and its implications for diterpenoid fragrance production. The Journal of biological chemistry. 287**,** 12121-31.

Zi, J., Matsuba, Y., Hong, Y., Jackson, A., Pichersky, E., Tantillo, D. J., Peters, R. J., 2014. Biosynthesis of lycosantalonol, a *cis*-prenyl derived diterpenoid. J. Am. Chem. Soc. 136**,** 16951-16953.